

High-Energy Cosmic Rays from Gamma-Ray Bursts

Stuart D. Wick,^{a,b} Charles D. Dermer,^a and Armen Atoyan^c

^a*Code 7653, Naval Research Laboratory, Washington, DC 20375-5352 U.S.A.*

^b*NRL/National Research Council Research Associate*

^c*CRM, Université de Montréal, Montréal, Canada H3C 3J7*

Abstract

A model is proposed for the origin of cosmic rays (CRs) from $\sim 10^{14}$ eV/nucleon to the highest energies ($\gtrsim 10^{20}$ eV). GRBs are assumed to inject CR protons and ions into the interstellar medium of star-forming galaxies—including the Milky Way—with a power-law spectrum extending to a maximum energy $\sim 10^{20}$ eV. The CR spectrum near the knee is fit with CRs trapped in the Galactic halo that were accelerated and injected by an earlier Galactic GRB. These CRs diffuse in the disk and halo of the Galaxy due to gyroresonant pitch-angle scattering with MHD turbulence in the Galaxy's magnetic field. The preliminary (2001) KASCADE data through the knee of the CR spectrum are fit by a model with energy-dependent propagation of CR ions from a single Galactic GRB. Ultra-high energy CRs (UHECRs), with energies above the ankle energy at $\gtrsim 3 \times 10^{18}$ eV, are assumed to propagate rectilinearly with their spectrum modified by photo-pion, photo-pair, and expansion losses. We fit the measured UHECR spectrum assuming comoving luminosity densities of GRB sources consistent with possible star formation rate histories of the universe.

For power-law CR proton injection spectra with injection number index $p \gtrsim 2$ and low and high-energy cutoffs, normalization to the local time- and space-averaged GRB luminosity density implies that if this model is correct, the nonthermal content in GRB blast waves is hadronically dominated by a factor ≈ 60 -200, limited in its upper value by energetic and spectral considerations. Calculations show that 100 TeV – 100 PeV neutrinos could be detected several times per year from all GRBs with kilometer-scale neutrino detectors such as IceCube, for GRB blast-wave Doppler factors $\delta \lesssim 200$. GLAST measurements of γ -ray components and cutoffs will constrain the product of the nonthermal baryon loading and radiative efficiency, limit the Doppler factor, and test this scenario.

Key words: Gamma Ray Bursts, Cosmic Rays, Gamma Rays, Neutrinos

1 Introduction

Advances on both observational and theoretical fronts start to bring the solution to the problem of cosmic-ray origin within reach. GRBs provide the necessary ingredients to explain CR origin at ultra-high energies (1; 2), and could make a significant contribution at all energies (3). Long-duration GRBs are observed only in galaxies undergoing active star formation (4), and are probably associated with core collapse of massive stars (5; 6). Supernova (SN) emissions in the GRB optical afterglow light curves indicate that GRBs are related to Type Ib/c SNe (7; 8). Strong and intense nonthermal radiations are measured from GRBs (9), demonstrating powerful particle acceleration by GRB outflows.

Recent high-energy CR studies give new clues about CR injection and transport. KASCADE measurements (10; 11; 12) of the energy spectra of different CR ionic species between ≈ 1 and 100 PeV show that the energies of the spectral breaks are proportional to ionic charge Z , so that CR ion spectra display a rigidity-dependent feature related either to production or transport. The knee energy of the CR spectrum at $E_K \cong 3$ PeV results from the spectral break of the dominant H and He species. Data from air fluorescence detectors (13) and air shower arrays (14) reveal detailed outlines of the CR spectrum to the highest energies, possibly indicating features related to the Greisen-Zatsepin-Kuzmin (GZK) suppression of the UHECR flux above $E \sim 6 \times 10^{19}$ eV (15; 16), where the energy-loss length of CR protons due to photopion losses equals the Hubble radius (see Ref. (17) for a review).

On the theoretical side, various processes that could be effective for accelerating particles to ultra-high energies have been identified in studies of collisionless shock acceleration. These include acceleration in colliding relativistic shells (2; 18), second-order gyroresonant acceleration in a relativistic shocked fluid (19), and a converter mechanism (20) for neutrals that can overcome difficulties (21) to accelerate CRs to ultra-high energies at external shocks (1). These difficulties are in any case ameliorated if the GRB takes place in a region of strong magnetic field such as a pulsar wind nebula (22; 23), or even in the magnetized wind of a massive-star collapsar progenitor. The important processes governing energy losses and secondary production of UHECRs are, moreover, now well understood (24; 25; 26).

In this paper we develop a model for high energy cosmic rays (HECRs; here defined as $\gtrsim 10^{14}$ eV/nucleon CRs), based on the underlying assumption that CRs are accelerated in the relativistic and nonrelativistic shocks found in GRBs and their attendant SNe. To test the model, KASCADE (12) and HiRes-I and HiRes-II Monocular data (13) are fit over the energy range $\approx 2 \times 10^{16}$ eV to $\approx 3 \times 10^{20}$ eV. A good fit to the entire data set is possible if CRs are

injected with a power-law spectrum with number index $p = 2.2$, as could be expected in a scenario where particles are accelerated by relativistic shocks (27; 28).

CRs that are injected with energies $\lesssim 10^{19}$ eV diffuse through and escape from their host galaxy. The sources of high-energy CRs, namely GRBs, are located in star-forming regions found in the galaxy’s disk. CR transport in the disk and halo of the Milky Way is modeled using a time-dependent, spherically-symmetric propagation model that employs an energy-dependent, spatially-independent diffusion coefficient. The random-walk pathlengths are assumed to arise from gyroresonant, pitch-angle scattering of CRs with a magnetohydrodynamic (MHD) turbulence spectra that can be decomposed into two components reflecting different power-law distributions of turbulence over different wavelength ranges. For a Kraichnan spectrum of MHD turbulence with index $q = 3/2$, the CR spectrum from an impulsive source is 0.75 units steeper than the injection spectrum. For a Kolmogorov spectrum of MHD turbulence, propagation effects steepen the injection spectrum of an impulsive source of CRs by 0.5 units. The spectral break at the CR knee energy is therefore explained in an impulsive, single-source model for HECRs if the turbulence spectral index changes from Kraichnan to Kolmogorov turbulence near the wavenumber resonant with CRs at the knee of the CR spectrum. We model the preliminary 2001 KASCADE data by assuming that all ionic species have the same injection index, with the compositions of the ions adjusted to fit the observed CR spectrum near the knee. Additional hardenings of the low-energy CR spectrum from a single GRB source of HECRs can result both from energy-dependent diffusion and from a low-energy cutoff in the CR injection spectrum.

Superposition of the contributions from many SNe are assumed to accelerate the bulk of the GeV/nuc – TeV/nuc CRs, as in the conventional scenario (29; 30). The derived diffusion properties of the ISM could indicate that the average injection index $\langle p \rangle \cong 2.4$ for these CR sources, because the mean CR spectrum from many sources is $1/3^{rd}$ power steeper than the injection index when CRs gyroresonantly diffuse through pitch-angle scatterings in a Kolmogorov spectrum of turbulence.

UHECRs have such large gyroradii and diffusion mean free paths that they are assumed to escape directly from the halo of the GRB host galaxy and stream into metagalactic space. The UHECR energy spectrum evolves in response to photo-pair and photo-pion losses on the redshift-dependent cosmic microwave background radiation (CMBR), which we treat in a continuous energy-loss formalism. UHECRs in intercluster space also lose energy adiabatically due to cosmic expansion. The measured UHECR spectrum arises from the contributions of sources throughout the universe, with an intensity that depends on the local luminosity density of GRB sources and the evolution of the GRB

luminosity density with redshift. The UHECR spectral model assumes that many sources produce the measured ultra-high energy and super-GZK ($\geq 10^{20}$ eV) CRs. Based on the local luminosity density of GRB sources and current estimates of the GRB beaming fraction (Section 2), a large number of GRBs would indeed occur within the photopion energy-loss radius for super-GZK CRs over a timescale of $\sim 100 \text{ Mpc}/c \sim 300 \text{ Myr}$.

Our model for UHECRs from GRBs implies a local time- and space-averaged CR luminosity density $\dot{\epsilon}_{CR} = f_{CR} \dot{\epsilon}_{GRB, X/\gamma}$ of CRs where the local ($z \ll 1$) luminosity density $\dot{\epsilon}_{GRB, X/\gamma} \approx 10^{44} \text{ ergs Mpc}^{-3} \text{ yr}^{-1}$ is inferred from BATSE observations of the hard X-ray/soft γ -ray (X/ γ) emission from GRBs (31; 32; 3). The value of $\dot{\epsilon}_{CR}$ depends sensitively on the minimum energy E_{min} of CR injection for soft injection spectral indices $p \gtrsim 2$. For $p \simeq 2.2$, if $E_{min} = 1 \text{ GeV}$ then $\gtrsim 700\times$ more energy must be injected in nonthermal hadrons than is observed as X/ γ emission from GRBs. If $E_{min} \approx 100 \text{ TeV}$, then $\approx 70\times$ more energy is required. Such large baryon loads would provide a bright cascade emission signature in GRB spectra at MeV – GeV energies through photopion or hadron synchrotron processes (33; 34). EGRET observations already constrain the product of nonthermal baryon-load and hadronic radiative efficiency, though it will require the *Gamma-ray Large Area Space Telescope*¹ (*GLAST*) to measure the ranges of spectral properties of GRBs at GeV energies.

The large nonthermal baryon load, $f_{CR} \gg 1$, required to fit the UHECR data assuming that the GRBs comoving luminosity density traces the star formation rate (SFR) history, implies that GRBs can be much more luminous neutrino sources than predicted under the standard assumption that the energy injected into a GRB blast wave in the form of CRs is equal to the energy inferred from X/ γ fluence measurements of GRBs (35). We therefore predict that if this model is correct, and CRs are accelerated and injected in the form of soft power-laws with index $p \gtrsim 2$, then IceCube should detect up to several neutrinos from the brightest GRBs with total X/ γ radiation fluence at levels $\gg 10^{-4} \text{ erg cm}^{-2}$. This prediction holds both in a collapsar scenario when the Lorentz factors Γ of the relativistic outflows are $\lesssim 200$, or if the GRB takes place in an intense external radiation background for a wide range of Γ . Lower limits to Γ can be inferred from γ -ray transparency arguments applied to observations of GRBs with GLAST.

We also consider whether this model can explain the AGASA data (14) for the UHECRs. Poor fits are found if GRBs inject soft CR spectra with $p \gtrsim 2$. However, if GRBs inject hard spectra with $p \approx 1$, for example, through a second-order relativistic shock-Fermi process (19) or through the converter mechanism (20), then the highest-energy AGASA data can be fit, though the

¹ <http://www-glast.stanford.edu/>

reduced χ^2 of our best fits are not compelling. Because the injection spectrum is so hard, most of the produced high-energy neutrinos are too energetic and the flux too weak to be detected with IceCube, though other telescope arrays, such as the Extreme Universe Space Observatory (EUSO), could be sensitive to these GZK neutrinos. To explain the CRs below $\approx 3 \times 10^{19}$ eV, an additional component of CRs would still be required either from GRBs or another class of sources, and these would make an additional contribution to high-energy neutrino production.

This work builds on the studies of Vietri (1995) and Waxman (1995), who proposed that UHECRs originate from GRBs (see also Ref. (36)), and begins to fill in details of the synthesis of CRs, SNe, and GRB sources proposed by Dermer (2002). Section 2 gives a more detailed description of the observational and theoretical basis for this model. Our propagation model describing CR diffusion in the disk and halo of the Galaxy is presented in Section 3, where we fit the KASCADE data between ≈ 0.8 and 200 PeV with a single Galactic GRB source ≈ 500 pc away that took place around 200,000 yrs ago. In Section 4, we describe our calculation of the UHECR flux, including energy losses from cosmic expansion, and photo-pair and photo-pion production. In Section 5, we present minimum χ_r^2 fits to the high-energy KASCADE, HiRes-I and HiRes-II Monocular data covering the energy range 2×10^{16} eV to 3×10^{20} eV. We also fit the AGASA data from 3×10^{19} eV to 3×10^{20} eV for hard CR injection spectra. Section 6 presents new high-energy neutrino calculations from hadronically dominated GRBs, and our predictions for km-scale high-energy neutrino telescopes such as IceCube or a deep underwater, northern hemisphere array. A discussion of the results is given in Section 7, and summary and conclusions are presented in Section 8.

2 Gamma Ray Burst Model for High-Energy Cosmic Rays

For reasons reviewed in Refs. (3), (37) and (38), the progenitor sources of HEERs are likely to be GRBs. The important clues are observational.

- (1) The evidence from KASCADE that the break energies of the different CR ionic species are proportional to rigidity, and that the mean atomic mass increases with E through the knee region, admits a propagation solution to understand the energies of the spectral breaks of different CR ions—given a galactic source that injects power-law CRs to the highest energies.
- (2) Composition changes above the “second knee” at $E \approx 10^{17.6}$ eV, and possible GZK features in the UHECR spectrum, implies that UHECRs and their sources are metagalactic.
- (3) The CR all-particle spectrum breaks at $\cong 3$ PeV by ≈ 0.3 units and then

extends without spectral change, other than for a possible weak softening above the second knee, to the ankle at $E \approx 3 \times 10^{18}$ eV (39). A single power-law injection source, modified by acceleration and transport effects, and energy losses in transport, provides the most economical solution from a mathematical standpoint, and allows one to derive the strongest constraints on the source properties and their environments.

- (4) A comprehensive model of HECRs therefore seems achievable if a source type that injected power-law distributions of relativistic CRs were found in star-forming L^* galaxies such as the Milky Way, with injection episodes frequent and energetic enough to power the HECRs.

Our current understanding of the long-duration GRBs converges to satisfy the requirements of observations. To summarize briefly, spectroscopic evidence connects GRBs to star-forming regions (4) and, consequently, to high-mass stars. GRB host galaxies have blue colors, consistent with galaxy types that are undergoing active star formation. GRB counterparts are found within the optical radii and central regions of the host galaxies (40). Lack of optical counterparts in some GRBs could be due to extreme reddening from large quantities of gas and dust in the host galaxy (41). Supernovae-like emissions have been detected in the late-time optical decay curves of a few GRBs (42; 43) and, most convincingly, in GRB 030329 (8). These observations show that, at least in these cases, GRBs are accompanied by a nearly contemporaneous SN that is spectrally much like the Type Ib/c SN 1998bw, which is temporally and spatially associated with GRB 980425 (7).

X-ray features have been detected in at least 6 GRBs, including variable Fe absorption during the γ -ray luminous phase of GRB 990705 (44), X-ray emission features in the afterglow spectra of GRB 991216 (45), low significance X-ray Fe K features observed in GRB 970508 (46), GRB 970828 (47), and GRB 000214 (48), and multiple high-ionization emission features detected in GRB 011211 (49). This indicates that GRBs take place in environments highly enriched in metals, such as active star-forming regions.

Taken together, the sources of GRBs appear to be a subset of SNe powered by the collapse to a black hole of a massive (\gtrsim several M_\odot) core stripped of its H and He envelope. The collapse event drives a subrelativistic outflow to power the SN, and a relativistic outflow to power the GRB. The GRB outflow is likely to be highly collimated. Possible stellar progenitor candidates are Wolf-Rayet stars (50), or merger events involving He cores (51). The earlier ejection of a stellar envelope would be advantageous to explain the X-ray features, as in the supranova model (52), but the evidence from the delayed reddened SN-like excesses favor a collapsar model (53) where a SN explosion accompanies the formation of the black hole that powers the GRB.

In the combined GRB/SN system currently envisioned, the marginally relativistic though energetic outflow associated with the SN and the highly relativistic outflow associated with the GRB blast wave provide very effective accelerators, as established from direct observations of GRB and SN Ib/c emissions. First-order (54) and second-order (19; 55) Fermi acceleration at the shocks associated with the marginally relativistic and strongly relativistic outflows gives rise to a power-law distribution. First-order shock acceleration in colliding relativistic shells (2; 18), and first-order Fermi acceleration at a relativistic external shock (27; 28), are each expected to inject a power-law distribution with number index $p > 2$ extending to $\gtrsim 10^{20}$ eV, though acceleration of UHECRs at an external shock could operate most effectively in the highly magnetized pulsar wind bubble environment of the supranova model (21; 56; 23). Low-energy cutoffs to the injection spectra can result from stochastic acceleration of a pre-existing particle population, or from the Γ^2 bounce that swept-up CRs receive at a relativistic shock (1), with very high-energy cutoffs potentially achievable in a proto-plerionic environment for particles that escape in the upstream direction (23).² In a variant of the first-order process, harder injection spectra occur when neutral intermediaries are formed and travel upstream, because this allows an upstream particle to execute a larger fraction of a cycle before recapture by the relativistic shock (20). Hard injection spectra ($p \approx 1$) with $E_{max} \gtrsim 10^{20}$ eV can be formed with second-order stochastic gyroresonant acceleration in the shocked fluid of a relativistic shock (19; 2). For reasons of acceleration efficiency and available power, GRBs are therefore strongly favored to be the sources of HECRs.

Gamma-ray astronomy was supposed to solve the cosmic-ray origin problem, but has as yet failed to do so (58). HEGRA results for the low-intensity flux (59) from Cas A indicate that most SNe are rather inefficient at accelerating GeV/nuc-TeV/nuc particles compared with earlier theoretical expectations. EGRET did not reveal emissions from SNR shells with compelling significance. CANGAROO results (60) are ambiguous (61). New results from HESS, VERITAS, GLAST, and multiwavelength studies of the unidentified EGRET sources will indicate whether a subset of SNRs are bright hadronic sources, as predicted in this scenario (3), with much less efficient CR acceleration in the slower Type II SN outflows.

Within this model, we do not dispute the conventional interpretation (29; 30; 62; 63; 64) that “ordinary” Type II and Type Ia SNe accelerate some significant and possibly dominant fraction of CRs with energies below the knee. Here we focus on the acceleration of HECRs in marginally relativistic SNe and highly relativistic GRB outflows, which offers several mechanisms to overcome the difficulties (65) with conventional first-order processes to accelerate CRs

² Γ is the bulk Lorentz factor of the relativistic outflow. We operate in a fire-ball/blastwave framework (57; 5).

to energies $\gtrsim 10^{14} Z$ eV in the shocks formed in Type II SNRs.

2.1 Local GRB and Super-GZK Emissivities

Two important issues must still be summarized before we develop our model for HECRs from GRBs. The first is the question of the claimed coincidence between the local ($z \ll 1$) time- and space-averaged GRB luminosity density (or emissivity) $\dot{\epsilon}_{GRB,X/\gamma}$ (ergs Mpc $^{-3}$ yr $^{-1}$) and the local luminosity density $\dot{\epsilon}_{GZK}$ required to power the super-GZK ($\geq 10^{20}$ eV) CRs. Pre-Beppo SAX estimates (1; 2) concerning the X/ γ emission from GRBs found

$$\dot{\epsilon}_{GRB,X/\gamma} \simeq 10^{44} \dot{\epsilon}_{44} \text{ ergs Mpc}^{-3} \text{ yr}^{-1}, \quad (1)$$

with $\dot{\epsilon}_{44} \approx \text{few}$. This exceeds the local ($z \ll 1$) GZK emissivity $\dot{\epsilon}_{GZK} \simeq u/t_{\phi\pi} \simeq 6 \times 10^{43} u_{-21} \text{ ergs Mpc}^{-3} \text{ yr}^{-1}$ required to power $> 10^{20}$ eV CRs, where $10^{-21} u_{-21} \text{ ergs cm}^{-3}$ is the observed energy density in $> 10^{20}$ eV CRs ($u_{-21} \cong 0.5$ for HiRes and $u_{-21} \cong 2$ for AGASA), and the photo-pion energy-loss timescale for a 10^{20} eV proton is $140 \text{ Mpc}/c$ (66). A better estimate that corrects for the energy-dependence of $t_{\phi\pi}$ implies $\dot{\epsilon}_{GZK} \simeq u/t_{\phi\pi} \simeq 10^{44} u_{-21} \text{ ergs Mpc}^{-3} \text{ yr}^{-1}$, comparable with the GRB emissivity $\dot{\epsilon}_{GRB,X/\gamma}$, so that the required luminosity density to power the super-GZK CRs is in coincidence with that available from GRBs.

With the advent of the Beppo-SAX results leading to redshift measurements of GRB counterparts, Stecker (67) pointed out that if the luminosity density of GRBs follow the SFR history of the universe, as implied by observations linking GRBs to massive stars, then $\dot{\epsilon}_{GRB,X/\gamma}$ could be a factor ~ 10 less than estimated by Waxman (2) and Vietri (1). Furthermore, the estimate strictly only applies to the long-duration GRBs—about 2/3rds of the total—for which we have distance estimates. Another point is that the most distant GRBs localized with Beppo-SAX are at redshifts $z \approx 4.5$ rather than unity, which could in principle reduce the local emissivity. Dermer (3) made the first quantitative estimate for the GRB luminosity density based on the study by Böttcher and Dermer (32) of BATSE statistics in the external shock model, and derived a value of $\dot{\epsilon}_{44} \cong 4$ using an analytic fit to the SFR derived from Hubble Deep Field measurements (93). This emissivity includes, in addition to the photon luminosity that is dominated by hard X-ray and γ -ray emission, an inefficiency factor for production of photons due to the radiative regime implied by the fits to the data (32), and a further correction for dirty and clean fireballs, which have since been discovered (68), as predicted (69).

Removing the inefficiency factor from the estimate of Ref. (3) gives the local GRB emissivity in the form of nonthermal photon radiation to be $\dot{\epsilon}_{44} \cong 0.6$.

Vietri, de Marco, and Guetta (23) argue for a value of $\dot{\epsilon}_{44} \cong 1.1$, taking into account bolometric corrections, though they say that this is “...the energy-release rate in gamma-ray photons.”

Given the various uncertainties, we take the local macroscopic GRB emissivity in the form of hard X-rays and 100 keV – MeV γ -rays from GRBs to be

$$\dot{\epsilon}_{44} \cong 1, \quad (2)$$

where future statistical studies of cosmological GRBs will be required to make more accurate calculations.

2.2 Beaming and GRB Rate

The second issue is the beaming and source rate.

Analysis (70) of beaming breaks in the optical light curves of GRBs indicate that the most apparently luminous GRBs are highly collimated. Frail et al. (71) argue that a typical GRB has a beaming factor of $1/500^{th}$ of the full sky, so that GRBs are in actual fact 500 times more numerous, and $1/500^{th}$ as energetic on average, as the measured energy releases imply. This means that most GRBs typically release $\approx 5 \times 10^{50}$ ergs in X/ γ emission.

The local density of L^* spiral galaxies, of which the Milky Way is representative, can be derived from the Schechter luminosity function, and is $\approx 1/(200-500 \text{ Mpc}^3)$ (72; 3). The BATSE observations imply ~ 2 GRBs/day over the full sky (73). Due to beaming, this rate is increased by a factor of $500f_{500}$, where $f_{500} \sim 1$. Given that the volume of the universe is $\sim 4\pi(4000 \text{ Mpc})^3/3$, this implies a rate per L^* galaxy of

$$\begin{aligned} \rho_{L^*} &\approx \frac{(200 - 500) \text{ Mpc}^3/L^*}{\frac{4\pi}{3}(4000 \text{ Mpc})^3} \frac{700}{\text{yr}} \times 500f_{500} \times SFR \times K_{FT} \\ &\approx (200 - 500) \frac{\text{Mpc}^3}{L^*} \times 0.33 \frac{\text{isotropic events}}{\text{Gpc}^3 \text{ yr}} \times 500f_{500} \times \left(\frac{SFR}{1/8}\right) \times K_{FT} \\ &\approx (1 - 3) \times 10^{-4} \left(\frac{SFR}{1/8}\right) \times \left(\frac{K_{FT}}{3}\right) \times f_{500} L^{*-1} \text{ yr}^{-1}. \end{aligned} \quad (3)$$

The factor SFR corrects for the star-formation activity at the present epoch [$SFR(z = 0) \cong (1/8)SFR(z = 1)$] (see Section 4), and the factor K_{FT} accounts for dirty and clean fireball transients that are not detected as GRBs (32). This estimate is in complete agreement with the result of Ref. (23) that

excludes short GRBs, based on Schmidt’s analysis (74) of the local GRB rate. Thus a GRB occurs about once every 3–10 millennia throughout the Milky Way, or at about 10% of the rate of Type Ib/c SNe.³

We write $\dot{\epsilon}_{CR} = f_{CR}\dot{\epsilon}_{GRB,X/\gamma}$ for the local luminosity density of CRs injected by GRBs, where f_{CR} is the nonthermal baryon-loading factor by which the emissivity injected by GRBs in the form of hadronic CRs exceeds the emissivity inferred from direct observations of the X/ γ emission from GRBs. In the following, we take $\dot{\epsilon}_{44} = 1$ (eq.2). From eqs. (3) and (1), we find that the average apparent isotropic energy release per GRB is $\cong 10^{53}(f_{CR} + \dot{\epsilon}_{44})/(K_{FT}/3)$ ergs, and the smaller actual mean energy release per GRB due to beaming and the consequent larger number of GRB sources is $\cong 2 \times 10^{50}(f_{CR} + \dot{\epsilon}_{44})/[f_{500}(K_{FT}/3)]$ ergs.

In principle, the nonthermal CR baryon-loading factor f_{CR} could be as large as $\approx 10^4$ when a Solar mass core is completely converted into nonthermal particles. An efficiency of $\sim 1\%$ seems more feasible, so that the actual GRB energy release in the form of CRs, E_{CR} , is $\approx 10^{52}$ ergs. For our canonical model GRB used to fit CR data near the knee, we take $E_{CR} = 10^{52}$ ergs, corresponding to $f_{CR} = 50$. A value of $f_{CR} \gtrsim 50$ is implied by the data fits if this model for HECRs is correct (Section 5). Hence, in a unified model for HECRs from GRBs, the GRB blast wave must be strongly baryon-loaded with $f_{CR} \gtrsim 50$ —at least during the prompt phase of the GRB when the acceleration is most rapid. This strong baryon-loading implies rates and numbers of events that are favorable for detection with a km-scale neutrino telescope such as IceCube.

This reasoning suggests a unified basis for understanding the origin of HECRs from GRBs and, by including the medium-energy CRs accelerated through the first-order Fermi mechanism in nonrelativistic SNR shocks powered by core collapse to a neutron star, a complete theory for the origin of the cosmic rays.

3 Galactic Cosmic Rays from GRBs

Because long-duration GRBs are associated with massive stars and Type Ib/c SNe (see Section 2), we suppose that GRB sources are located in the disks and star-forming regions of galaxies undergoing active star formation. The relativistic ejecta in the GRB explosions accelerate and inject CRs into the ISM of the GRB host galaxy in the form of a power law to the highest energies,

³ The possible inclusion of a GRB population related to Type II-p SNe would likely not increase this rate by more than a factor of $\sim 50\%$ (A. Fillipenko, private communication, 2003).

though possibly with a low-energy cutoff to the accelerated proton spectrum. In relativistic blast waves, this cutoff is expected at $\sim \Gamma^2$ GeV energies, which could easily reach TeV – PeV energies for typical GRB blast waves with $\Gamma \sim 10^2 - 300$. UHECR acceleration and injection probably occurs during the γ -ray luminous phase of a GRB, which is on the order of minutes to hours. Acceleration and injection of lower energy CRs might operate on the Sedov time scale, which could exceed thousands of years. These acceleration times are still short compared to the times for particles with the corresponding energies to diffuse a distance comparable to the disk scale height, as can be shown from the diffusion properties of the Galaxy derived below. A GRB source can therefore be treated as an impulsive source of CR injection.

In this section we present a simplified propagation model for CRs in the disk and halo of the Galaxy.

3.1 Diffusion Mean Free Path

We assume that the Galaxy's disk magnetic field consists of a large-scale field of mean strength $B = B_{\mu G} \mu G$ on which is superposed a spectrum of MHD turbulence. The diffusion mean-free-path λ for CRs diffusing through this field is a function of the Larmor radius

$$r_L = \frac{Am_p c^2 \beta \gamma}{ZeB} \sin \alpha \cong \frac{E}{QB} \cong 3.12 \times 10^{12} \frac{A\gamma}{ZB_{\mu G}} \text{ cm} \cong \frac{A\gamma_6}{ZB_{\mu G}} \text{ pc} , \quad (4)$$

where $\gamma = 10^6 \gamma_6$ is the Lorentz factor of the relativistic CR proton or ion with atomic mass A , $\beta = \sqrt{1 - \gamma^{-2}}$, and the pitch angle α is set equal to $\pi/2$. We assume isotropic turbulence, though it is straightforward to generalize the treatment for particle-scattering properties that differ in directions parallel and transverse to the plane of the disk.

We consider a very simplified approach to CR transport where particles diffuse via pitch-angle scattering with resonant MHD turbulence; see, e.g., Refs. (75; 76; 77), and Ref. (64) for a detailed treatment. Let $w(k)dk$ represent the differential energy density of isotropic MHD turbulence with wavenumbers between k and $k + dk$. We first consider the case where the MHD turbulence spectrum is described in the inertial range by a single power-law function $kw(k) = w_0(k/k_1)^{1-q} H(k; k_1, k_2)$, where $H(x; a, b) = 1$ when $a \leq x \leq b$ and $H(x; a, b) = 0$ otherwise, and q is the spectral index of the wave spectrum. The index $q = 5/3$ for a Kolmogorov spectrum of turbulence, $q = 3/2$ for a Kraichnan spectrum of turbulence (see Ref. (78)), and $w_{tot} = w_0/(q - 1)$ is the total energy density of MHD turbulence when $q > 1$ and $k_2 \gg k_1$. Note that this description of the wave turbulence is an extreme oversimplification,

insofar as we do not consider different wave modes and helicities, or distinguish between forward- and backward-propagating waves.

The ratio of the MHD wave energy w_{tot} to the energy density $U_B \equiv B^2/8\pi$ of the large-scale component of the Galactic magnetic field is denoted by ξ_1 , so that $kw(k) \cong (q-1)\xi_1 U_B (k/k_1)^{1-q}$ for $k_1 \leq k \leq k_2$. The value of k_1 corresponds to the inverse of the largest size scale on which turbulence is injected.

We make the ansatz that the diffusion coefficient of a CR with Larmor radius r_L is inversely proportional to the energy density in gyroresonant waves with wavenumber $\bar{k} \sim r_L^{-1}$ (79). This gyroresonance condition is a simplification of the more general condition $\omega - k_{\parallel}v_{\parallel} = cl/r_L$, where ω is the wave frequency, k_{\parallel} and v_{\parallel} are the wave number and particle speed parallel to the large-scale magnetic field direction, and l is an integer (76; 80). (Protons and ions resonate with shear Alfvén waves via the $l = +1$ mode and fast mode waves via the $l = -1$ mode.) We therefore have $\lambda = r_L U_B / \bar{k}w(\bar{k}) = k_1^{1-q} r_L^{2-q} / \xi_1 (q-1) = b_1^{q-1} r_L^{2-q} / \xi_1 (q-1) \propto \gamma^{2-q}$, giving

$$\lambda(\text{pc}) = \frac{b_{pc}^{q-1}}{(q-1)\xi_1} \left(\frac{A\gamma_6}{ZB_{\mu\text{G}}} \right)^{2-q} = \begin{cases} \frac{3b_{pc}^{2/3}}{2\xi_1} \left(\frac{A\gamma_6}{ZB_{\mu\text{G}}} \right)^{1/3}, & \text{for } q = 5/3 \\ \frac{2b_{pc}^{1/2}}{\xi_1} \left(\frac{A\gamma_6}{ZB_{\mu\text{G}}} \right)^{1/2}, & \text{for } q = 3/2 \end{cases}, \quad (5)$$

where $k_1 = 1/b_1 = b_{pc}^{-1} \text{ pc}^{-1}$.

Equation (5) gives the mean-free path λ of relativistic ($\gamma \gg 1$) CRs that diffuse due to gyroresonant interactions with large-wavenumber ($k > k_1$) turbulence. When $r_L^{-1} < k_1$, or $r_L > b_{pc} \text{ pc}$, CRs gyroresonate with small-wavenumber ($k < k_1$) turbulence. If the knee in the CR all-particle spectrum at $E_K \cong 3 \text{ PeV}$ is due to propagation effects, then $b_{pc} \cong 1$ when $B_{\mu\text{G}} = 3$ for the dominant CR proton species. The break energies in the spectra of other CR ions are also given by the relation $r_L = k_1^{-1}$, so that the knee energies for the different CR ions occur at energies

$$E_Z(\text{PeV}) \cong A\gamma_6 \cong ZB_{\mu\text{G}}b_{pc}. \quad (6)$$

The fit to the data described below uses $b_{pc} = 1.6 \text{ pc}$ and $B_{\mu\text{G}} = 3$. If the value of ξ_1 , corresponding to the ratio of the energy density $k \gtrsim k_1$ turbulence to U_B is a few percent, then $\lambda \simeq h_d$ for $\approx 3 \text{ PeV}$ CR protons, where h_d is the scale height of molecular gas or massive stars in the disk of the Milky Way. A break in the all-particle spectrum due to a change in the propagation mode occurs at $\approx 3 \text{ PeV}$, where $\lambda \approx h_d$, with a pattern of break energies $E_{br} \propto Z$ for the ionic constituents of the CR all-particle spectrum.

Although a CR proton with energy E_K has $r_L \sim \text{pc} \ll h_d$, its mean-free-path $\lambda(E_K) \sim h_d \gg r_L(E_K)$ because pitch-angle scattering results only from gyroresonant interactions with MHD waves that constitute a small fraction of the total magnetic field energy density. CRs injected with $E \gg E_K$ will diffuse through the Galaxy's disk and halo through gyroresonant pitch-angle scattering with MHD turbulence carried by waves with wavenumbers $k \ll k_1$ that gyroresonate with particles with $E \gg E_K$. This suggests that we consider a more general wave spectrum over a larger range of k given by the expression

$$kw(k) = A_0[f_H (\frac{k}{k_1})^{1-q_H} H(k; k_0, k_1) + (\frac{k}{k_1})^{1-q} H(k; k_1, k_2)] , \quad (7)$$

where q_H is the index of the small wavenumber MHD turbulence, and f_H normalizes the energy densities of the small ($k < k_1$) and large ($k > k_1$) wavenumber turbulence spectra at $k = k_1$. The normalization condition $\xi U_B = \int_0^\infty dk w(k)$ implies $A_0 = \xi U_B/g$, where

$$g = f_H \frac{[(\frac{k_1}{k_0})^{q_H-1} - 1]}{q_H - 1} + \frac{[1 - (\frac{k_2}{k_1})^{1-q}]}{(q - 1)} \approx \frac{f_H}{q_H - 1} (\frac{k_1}{k_0})^{q_H-1} + (q - 1)^{-1}. \quad (8)$$

The wave spectrum from eq. (7) is plotted in Fig. 1 by the solid lines. The parameters are $k_0 = 1/100 \text{ pc}^{-1}$, $k_1 = 1/1.6 \text{ pc}^{-1}$, $f_H = 0.2$, $\xi = 0.1$, $q_H = 3/2$, $q = 5/3$, and $B = 3\mu\text{G}$. Sixty-five percent of the turbulence energy density is in the small wavenumber component, so that $\xi_1 = 0.035$. The sharp edges in this wave spectrum introduce unphysically sharp features in the spectra of particles for this simple model of transport. A more physically plausible turbulence spectrum that retains the features of eq. (7) but smooths the particle distribution function, as would be physically expected from 3-wave interactions and turbulence-energy diffusion and cascading (81), is given by

$$kw(k) = f_H A_0 (\frac{k}{k_1})^{1-q_H} \Lambda_\Delta(\frac{k}{k_1}) [1 - \Lambda_\Delta(\frac{k}{k_0})] + A_0 (\frac{k}{k_1})^{1-q} [1 - \Lambda_\Delta(\frac{k}{k_1})], \quad (9)$$

where the smoothing function $\Lambda_\Delta(x) = \exp(-x^{-\Delta})$, and we let $k_2 \rightarrow \infty$. Eq.(9) reduces to eq. (7) in the limit $\Delta \gg 1$. Fig. 1 shows a plot of eq. (9) with $\Delta = 1.5$ and, for comparison, $\Delta = 6$. The subsequent fits to the data use the MHD wave spectrum, eq. (9), with $\Delta = 1.5$.

The ansatz $\lambda = r_L [U_B/\bar{k}w(\bar{k})]$ with $\bar{k} \rightarrow r_L^{-1}$ therefore implies

$$\lambda \cong (\frac{g}{\xi}) \frac{r_L}{f_H (r_L k_1)^{q_H-1} \Lambda_\Delta(r_L k_1) [1 - \Lambda_\Delta(r_L k_0)] + (r_L k_1)^{q-1} [1 - \Lambda_\Delta(r_L k_1)]}. \quad (10)$$

In Fig. 2, we plot λ and r_L as a function of total energy E for CR protons and Fe nuclei. The turbulence spectrum is given by Fig. 1 with $\Delta = 1.5$. Note

that $\lambda \cong 10$ kpc when the CR proton energy $E \approx 4 \times 10^{17}$ eV. This energy is near the onset of quasi-rectilinear propagation in a Galactic halo of size ≈ 10 kpc, and we expect a cutoff in the CR proton flux from a recent GRB in this energy range whenever we are not in the beam of a GRB jet (which is nearly always true because of the extreme improbability of such an occurrence). The energy-dependent cutoff will be $\propto Z$, as observed. The actual situation is of course more complicated due to the magnetic field gradient from the disk to the halo and on into metagalactic space.

3.2 Three Dimensional Isotropic Diffusion

We assume that a GRB injects a total energy $E_{CR} = 10^{52} E_{52}$ ergs in the form of cosmic rays. For impulsive injection, the number injection spectrum of CRs with atomic charge Z and atomic mass A is assumed to be given by $N_{Z,A}(\gamma) = c_{Z,A} K (\beta\gamma)^{-p}$ for $(\beta\gamma)_{min} \leq \beta\gamma \leq (\beta\gamma)_{max}$, and we assume that p is the same for all (Z, A) . When $(\beta\gamma)_{min} \ll 1$, $(\beta\gamma)_{max} \gg 1$, and $2 < p < 3$,

$$K \cong [1 + \frac{p-2}{2(3-p)}]^{-1} \frac{(p-2)E_{CR}}{m_p c^2 \sum_{Z,A} A c_{Z,A}}. \quad (11)$$

If $1 \ll (\beta\gamma)_{min} \cong \gamma_{min} \ll (\beta\gamma)_{max}$, $2 < p < 3$,

$$K \cong \frac{(p-2)E_{CR}\gamma_{min}^{p-2}}{m_p c^2 \sum_{Z,A} A c_{Z,A}}. \quad (12)$$

Cosmic rays are assumed to diffuse isotropically in the interstellar medium, with the initial anisotropy from injection by the GRB jet quickly washed out. For energy-dependent diffusive propagation, the spectral number density of relativistic CR ions with charge Z and mass A measured at a distance $r = 500 r_{500}$ pc away from an impulsive source of CRs from a GRB that occurred a time t earlier is

$$n_{Z,A}(\gamma; r, t) = \frac{c_{Z,A} K \gamma^{-p}}{\pi^{3/2} r_{dif}^3} \exp[-(r/r_{dif})^2]. \quad (13)$$

Here the diffusion radius $r_{dif} \cong 2\sqrt{D(\gamma)t} = 2\sqrt{\lambda ct/3}$, and eq. (13) assumes that CRs suffer no significant energy losses during transport (see Ref. (82) for the more general case).

Inspection of eq. (13) shows that when the observer is within the diffusion radius, that is, when $r \ll r_{dif}$, then

$$n_{Z,A}(\gamma; r, t) \propto \frac{\gamma^{-p}}{r_{dif}^3} \propto \frac{\gamma^{-p-\frac{3}{2}(2-q)}}{t^{3/2}} \propto t^{-3/2} \times \begin{cases} \gamma^{-p-\frac{1}{2}}, & \text{for } q = 5/3 \\ \gamma^{-p-\frac{3}{4}}, & \text{for } q = 3/2 \end{cases}. \quad (14)$$

The measured spectrum from a burstlike source is therefore steepened by $\frac{3}{2}(2-q)$ units, where the diffusion coefficient $D \propto \lambda \propto \gamma^{2-q}$ (82). (By comparison, the spectral index is steepened by $(2-q)$ units for continuous injection sources of CRs.) Eq. (14) shows that energy-dependent diffusion due to pitch-angle scattering with a Kolmogorov and Kraichnan spectrum of MHD turbulence steepens the injection spectrum of an impulsive source by 0.5 and 0.75 units, respectively. If the disk and halo magnetic fields of the Galaxy support a two-component MHD turbulence spectrum with indices $q = 5/3$ and $q_H = 3/2$, then an injection spectrum with $p = 2.2$ will be steepened to a measured spectrum $n_{Z,A}(\gamma; r, t) \propto \gamma^{-s}$, with $s = 2.7$ at $E \ll E_K$ and $s = 2.95$ at $E \gg E_K$. Because these indices are similar to the measured CR indices below and above the knee energy, we adopt this simplified model for CR transport. Speculations concerning the origin of such a turbulence spectrum are deferred to Section 7.

Fig. 3 shows the CR proton and Fe flux at different times after a GRB explosion located 500 pc from Earth. The low-energy cutoff energy is given by $(\beta\gamma)_{min} \ll 1$, so that most of the energy is deposited by ≈ 1 GeV/nuc CRs. When $(\beta\gamma)_{min} = (\beta\gamma)_{min,1} \gg 1$, the CR intensity is increased at energies above the low-energy cutoff by the factor $[(\beta\gamma)_{min,1}]^{p-2}$.

The flux of relativistic CRs is calculated from the expression

$$I_{Z,A}(E)(\text{m}^2 \text{ s sr GeV})^{-1} = \frac{10^4 c}{4\pi E(\text{GeV})} \gamma n_{Z,A}(\gamma; r, t), \quad (15)$$

where $E = \gamma A m_p c^2$ and $n_{Z,A}$ is in cgs units. Propagation effects arising from the combined disk and halo MHD turbulence spectrum produce a break in the spectrum at $E \approx 3$ PeV. The index of the CR number fluxes above the knee is ≈ 3.0 , for the reasons given above, until propagation effects at the “second knee” at $E \approx 4 \times 10^{17}$ eV start to soften the spectrum so that the metagalactic component begins to make a dominant contribution.

The observer is within the diffusion radius when $r_{dif}(\gamma) \cong 2\sqrt{D(\gamma)t} \gg r$, or when $ct \gtrsim r^2/\lambda$. If we are considering CRs with energies below the knee, then these particles scatter with the large wavenumber $k > k_1$, $q = 5/3$ turbulence, so that $\lambda \cong g k_1^{1-q} r_L^{2-q}/\xi$, where g is given by eq. (8). We write

$ct = 3.07 \times 10^5 t_{Myr}$ pc, where the observer is irradiated by a CR flux from a GRB that took place t_{Myr} Myr ago. At early times following the GRB, the low-energy portion of the measured CR spectrum from a GRB source is exponentially attenuated due to the slower diffusion of lower energy CRs. The observer will see the maximum flux from CRs with energies $E = Am_p c^2 \gamma$ when

$$t_{Myr} \approx 0.6 \left(\frac{\xi}{g}\right) r_{500}^2 \frac{1}{b_{pc}^{2/3}} \left(\frac{A\gamma_6}{ZB_{\mu G}}\right)^{-1/3} \approx 0.014 r_{500}^2 \left(\frac{A\gamma_6}{ZB_{\mu G}}\right)^{-1/3} . \quad (16)$$

This expression uses the parameters for the model fits discussed below, with $\xi = 0.1$ and $g \cong 4.3$, thus showing that the maximum flux of CR protons near the knee energy reaches an observer 500 pc away ≈ 14000 years after the GRB, in accord with Fig. 3. Eq. (16) shows that the low-energy cutoff γ_{cutoff} of the CR proton flux in Fig. 3 evolves according to the relation $\gamma_{cutoff} \propto r^{1/(1-q/2)} t^{-1/(2-q)}$. Note that eq. (16) is only valid when $t > r/c$.

Fits to the CR data near the knee are compatible with a 500 pc distant GRB releasing 10^{52} ergs in cosmic rays if the GRB took place $\approx 10^5$ yrs ago. This implies that the 0.1 – 100 PeV CR fluxes were up to 100 times brighter one or two hundred thousand years ago than they are today, though no test of this implication suggests itself.

3.3 Fits to the KASCADE Data

We now apply this model to fit the preliminary KASCADE data announced in 2001 (10; 11; 12). The points in Fig. 4 show KASCADE data and error bars for CR protons, He, Carbon, Fe, and the all-particle spectrum in panels (a) – (e), respectively. Fig. 4(d) also shows the reported 1σ boundary to the estimated systematic errors for CR Fe.

The fits to the KASCADE data shown in Fig. 4 use the propagation model previously described, with a GRB source of CRs at a distance $r = 500$ pc that exploded 210,000 yrs ago. The change in the diffusion and propagation properties leads to a break in the CR particle spectrum at break energies $\propto Z$ (eqs. [5] and [6]). Because of the preliminary nature of the data and the potentially significant systematic errors that could still remain in the early analyses, we did not perform a rigorous fit to the data, but instead adjusted the wavenumber k_1 and the compositions of the different ionic species until a reasonable fit to the data was obtained. With $B = 3\mu G$, the best value for the energy-dependent break was obtained with $k_1 \cong 1/1.6$ pc in the spectrum of turbulence.

The Anders-Grevesse Solar photospheric composition (83), and the (energy-

Table 1

Cosmic Ray Abundances Relative to Solar Photospheric Abundances (83)

Ion	$c_{Z,A}$	Enhancement
^1_1H	1.00	1.0
^4_2He	0.098	1.6
$^{12}_6\text{C}$	3.63×10^{-4}	50
$^{16}_8\text{O}$	8.51×10^{-4}	$\lesssim 5$
$^{56}_{26}\text{Fe}$	4.68×10^{-5}	20

independent) metallicity enhancements, compared to the Anders-Grevesse compositions, that were used to fit the data, are listed in Table 1. The strong enhancements by a factor of 50 and 20 for C and Fe, respectively, may be possible from highly-enriched winds that could be peculiar to a GRB stellar progenitor, or if there was an earlier supernova as in the supranova model. Note that O cannot be strongly enhanced if we are to maintain a good fit to the all-particle spectrum. A more detailed discussion about implications from composition will depend on fits to final analysis of KASCADE data (84).

As can be seen from Fig. 4, this model gives a reasonable fit to the data for the CR ion and all-particle spectra around the knee. Thus we argue that propagation effects from CRs injected and accelerated by a single GRB are responsible for the shape of the CR spectrum between ≈ 1 and 100 PeV.

This model must not overproduce CRs at energies below the knee. Fig. (5) compares CR observations with a model that fits the KASCADE data and has an injection momentum at $(\beta\gamma)_{min} = 0.01$. This model weakly overproduces the CR Carbon ions, though it is not a serious discrepancy given the uncertainty in the KASCADE data which determines the CR Carbon composition. A strong overproduction would imply a low-energy cutoff in the energy of the injected cosmic rays, or an earlier GRB. A model with a low-energy cutoff at 10^5 GeV would certainly be consistent with the medium-energy cosmic rays. In the proposed scenario, SN contributions to CR production make up the difference between CRs produced by a single GRB source and the measured CR fluxes below ≈ 100 TeV/nuc. The transition from multiple SNs source to, primarily, a single source seems to occur at energies of $\sim 1 - 100$ TeV/nuc.

3.4 Probability of Nearby GRB and CR Anisotropy

We estimate the probability that we find ourselves in the midst of a CR bubble formed by a recent, nearby GRB using the relation $P \simeq (r_{dif}/r_{MW})^2 N_{GRB}$.

The quantity $(r_{dif}/r_{MW})^2$ measures the relative area of the Milky Way's disk covered by a CR bubble with age t , and N_{GRB} is the number of GRBs that would have taken place during t . We normalize the rate of GRBs in the Milky Way to \dot{N}_M GRBs per millennium, and $\dot{N}_M \approx 0.1\text{--}0.3$ (Section 2). Thus $N_{GRB} = \dot{N}_{GRB}t = 10^3 \dot{N}_M t_{Myr}$.

Using model parameters, $r_{dif} = 2\sqrt{\lambda ct/3} \cong 4.9 t_{Myr}^{1/2} (A\gamma_6/ZB_{\mu G})^{1/6}$ kpc. Most of the active star formation in the Milky Way takes place within the spiral arms found within $r_{MW} = 15r_{15}$ kpc. Thus $P \simeq 106(t_{Myr}/r_{15})^2 \dot{N}_M (A\gamma_6/ZB_{\mu G})^{1/3}$, and the probability is very unlikely when $P(\bar{t}_{Myr}) \ll 1$, or when $t_{Myr} \lesssim \bar{t}_{Myr} \cong 0.1r_{15}\dot{N}_M^{-1/2} (A\gamma_6/ZB_{\mu G})^{-1/6}$. The model fits use a time of 0.21 Myr since the GRB exploded to fit the CR data, so there is a reasonable probability for this event to have taken place, even with $\dot{N}_M \approx 0.1$.

CRs from a GRB event that occurred much earlier than 0.2 Myr cannot fit the data unless the total energy release in CRs from a single GRB is increased, which makes severe demands on GRB models (see Fig. 3). For the estimated values of the diffusion coefficient, CRs from a GRB that occurred much later than ≈ 1 Myr also makes severe energy demands on the GRB source. Thus a GRB event occurring a few hundreds of millennia ago represents the most probable situation.

The anisotropy $\omega = (I_{max} - I_{min})/(I_{max} + I_{min}) = (3D/cn_{Z,A})(\partial n_{Z,A}/\partial r) = (\lambda/n_{Z,A})(\partial n_{Z,A}/\partial r)$ (87). Substituting eq. (13) gives

$$\omega = \frac{2r\lambda}{r_{dif}^2} = \frac{3}{2} \frac{r}{ct} \cong \frac{0.2r_{500}}{t_{Myr}}\%.$$
 (17)

The interesting point about eq. (17) is that ω is independent of energy for this diffusion model.

Analyses of the arrival directions of large numbers of CRs show anisotropies near 3 PeV at the $\approx 0.15 \pm 0.05\%$ level (88; 89). When E is between 100 GeV and 100 TeV, anisotropies of $\simeq 0.1\%$ are found. Schlickieser (64) discusses some sources of uncertainty in anisotropy measurements. An anisotropy of $\approx 1\%$ is implied from eq. (17) for $t_{Myr} = 0.21$. If an anisotropy below $\approx 0.2\%$ is confirmed, then a number of implications follow. Either we are located near a rather recent GRB, which could be unlikely, or the CR energy release from GRBs is larger than given here. Moreover, there could be contributions from a second GRB that would help isotropize the flux. Indeed, CR contributions from a multitude of weaker SNe that do not host GRBs could also help isotropize the CR flux. We discuss the relative contributions of SNe to the CR spectrum in Section 7.

4 Ultra-High Energy Cosmic Rays from GRBs

At energies greater than the knee in the cosmic-ray all-particle spectrum (~ 3 PeV), the spectral index steepens from ~ 2.7 to ~ 3.0 and continues as a power law until the spectrum steepens further to ~ 3.3 at the second knee ($\sim 4 \times 10^{17}$ eV). At the ankle ($\sim 3 \times 10^{18}$ eV), the spectrum hardens until an apparent pile-up appears at $\approx 5 \times 10^{19}$ eV. The spectrum has been measured to extend beyond 10^{20} eV with the highest-energy event to date of 3.2×10^{20} eV detected by the Fly's Eye Collaboration (90).

Soon after the discovery of the CMBR, it was pointed out by Greisen (91), and separately by Zatsepin and Kuzmin (92), that a proton with energy $E_p \gtrsim 5 \times 10^{19}$ eV will reach the threshold for pion production in proton-CMBR scattering and scatter within a Hubble time. The attenuation length for this process is $\simeq 140(15)$ Mpc for protons of energy $\simeq 10^{20}(10^{21})$ eV, as shown by (66) and our calculations below. Thus, a CR proton measured at $E_p \gtrsim 10^{20}$ eV must have originated from a distance $\lesssim 100$ Mpc (the GZK-distance). The GZK-effect predicts a suppression of the UHECR flux above $E_p \gtrsim 10^{20}$ eV.

The possibility that $\gtrsim 10^{20}$ eV protons could have been produced at cosmological distances with much higher energies is untenable given that the GZK-effect becomes more severe at earlier cosmic epochs, insofar as the CMBR temperature scales $\propto (1+z)$ and the CMBR number density increases $\propto (1+z)^3$. The presence or absence of the GZK-cutoff is currently an open question, and a subject of much interest to the astroparticle physics community. A violation of the cutoff implies either new physics or nearby astrophysical sources capable of accelerating CRs to super-GZK energies, albeit without disrupting the near isotropy of the observed flux. The experimental validation (or violation) of the GZK-cutoff should be resolved in the next generation CR measurements with the Auger Observatory.⁴

In our model the UHE component of the CR spectrum is produced by extragalactic GRBs. A clue that GRBs are a viable UHECR source comes from a comparison of the GRB luminosity density measured in γ -rays to that observed in the UHECRs (Section 2.1). Throughout our UHECR calculations we take the local GRB luminosity density in CRs to be

$$\dot{\epsilon}_{CR} = f_{CR} \dot{\epsilon}_{GRB,X/\gamma} \quad (18)$$

where $\dot{\epsilon}_{GRB,X/\gamma}$ is given in eqs.1 and 2 and f_{CR} is a parameter we vary to fit the UHECR data. The values of $\dot{\epsilon}_{CR}$ implied by the UHECR flux determines the nonthermal baryon-loading fraction f_{CR} required by a GRB model of HEERs.

⁴ <http://www.auger.org>

We assume that the GRB cosmic rate-density evolution, in comoving coordinates, follows the SFR history (93) derived from the blue and UV luminosity density of distant galaxies, with an analytic fitting profile given by

$$n(z) = n(0) \frac{1 + a_1}{(1 + z)^{-a_2} + a_1(1 + z)^{a_3}} \quad (19)$$

(37), where $n(z)$ is the GRB comoving rate density at epoch z . To accommodate present uncertainty in the true SFR evolution we take two models with $a_1 = 0.005(0.0001)$, $a_2 = 3.3(4.0)$, and $a_3 = 3.0(3.0)$ in line with the extreme ranges of optical/UV measurements without (with) dust extinction corrections. The lower optical/UV curve is arguably a lower limit to the SFR evolution, while a much stronger evolution of the SFR is found by Blain et al. (94) after correcting for dust extinction. To study the significance of this uncertainty in the measured UHECR flux, we therefore consider a “lower SFR” and “upper SFR” in each of our model fits. We plot these SFR histories in Fig. 6 in comparison with an oversimplified $n(z) = n(0)(1 + z)^4$ evolution used by other authors (102; 103), who perform similar UHECR calculations.

As is evident from Fig. 6, even our upper SFR evolution is seen to differ significantly from the SFR evolution $\propto (1 + z)^4$, when $z \gtrsim 2$. For $> 10^{20}$ eV CRs, this difference is irrelevant as all of these CRs must have originated from $z \ll 1$ due to severe CR attenuation during propagation, but the differing SFRs have an important effect on the predicted CR flux at energies $\lesssim 10^{18}$ eV due to photopair production.

Recent results from the Wilkinson Microwave Anisotropy Probe (104), in combination with other data, constrain the total energy density of the Universe to be $\Omega_{tot} = 1.02 \pm 0.02$ (105), in units of the closure density

$$\rho_c \equiv \frac{3H_0^2}{8\pi G} = 1.88 \times 10^{-29} h^2 \text{gm cm}^{-3}. \quad (20)$$

The value of the Hubble constant today is $H_0 = 100h \text{ km s}^{-1} \text{ Mpc}^{-1}$, where (105) find $h = 0.72 \pm 0.05$ and the fraction of the closure density in matter $\Omega_m = 0.27 \pm 0.04$. The High- z Supernova Search Team, measuring Type-1a supernovae in the redshift interval 0.3 to 1.2, constrain the dark energy density to $\Omega_\Lambda = 0.73 \pm 0.20$ assuming a dark energy equation-of-state with $w = -1$ (106). In keeping with these observational results, we adopt a Λ -cold dark matter (Λ CDM) cosmology where $\Omega_{tot} = 1.0$, $\Omega_m = 0.3$, and $\Omega_\Lambda = 0.7$, assuming a dark energy equation of state with $w = -1$ and $h = 0.7$.

4.1 CR Attenuation

We approximate the UHE protons as propagating rectilinearly. The Larmor radius of a UHE proton is $\simeq 100 E_{20}/B_{\mu\text{G}}$ kpc for a proton of energy $E = 10^{20} E_{20}$ eV propagating through a magnetic field of strength $B = B_{\mu\text{G}} \mu\text{G}$. In this approximation, the observed UHECR spectrum is that of the spectrum at the source modified by energy losses the proton suffers during propagation. At high energies, three processes dominate the proton's energy losses during propagation. They are 1) adiabatic expansion of the universe (i.e., red-shifting of the proton momentum), 2) electron-pair production from proton scattering on the CMBR ($p \gamma \rightarrow p e^+ e^-$), and 3) pion production from proton-CMBR scattering ($p \gamma \rightarrow \pi^+ n$). We describe our treatment of each of these processes below.

The expansion of the universe causes a red-shifting of the momentum of any propagating particle. This energy loss is

$$-\frac{1}{E} \frac{dE(z)}{dt} = \frac{1}{(1+z)} \frac{dz}{dt} \quad (21)$$

where for a ΛCDM cosmology,

$$\frac{dz}{dt} = (1+z) H_0 \sqrt{\Omega_m (1+z)^3 + \Omega_\Lambda} . \quad (22)$$

The fractional energy-loss rate of a proton scattering on CMBR photons is given by

$$-\frac{1}{E} \frac{dE(z)}{dt} = \int_{\epsilon_{th}/2\gamma_p}^{\infty} d\epsilon \frac{n_\gamma(\epsilon, z)}{2\gamma_p^2 \epsilon^2} \int_{\epsilon_{th}}^{2\gamma_p \epsilon} d\epsilon_r \sigma_{p\gamma}(\epsilon_r) K_{p\gamma}(\epsilon_r) \epsilon_r \quad (23)$$

(25), where $n_\gamma(\epsilon, z)$ is the black-body photon distribution of the CMBR with red-shift dependent temperature $T(z) = 2.72\text{K} (1+z)$, $\sigma_{p\gamma}(\epsilon_r)$ is the cross-section for the process at hand, and $K_{p\gamma}(\epsilon_r)$ is the proton inelasticity per interaction. The mean-free-path between scatterings is found from eq. (23) by setting $K_{p\gamma}(\epsilon_r) = 1$ for all ϵ_r .

Our treatment of energy losses from pion production follows Ref. (107), modified to include a three step cross-section and inelasticity function. The ap-

proximations that we use throughout for the photopion cross section are

$$\sigma_{p\gamma}(\epsilon_r) = \begin{cases} 40 \text{ mb} , & \text{for } 150 \text{ MeV} \leq \epsilon_r < 220 \text{ MeV} \\ 300 \text{ mb} , & \text{for } 220 \text{ MeV} \leq \epsilon_r < 450 \text{ MeV} \\ 110 \text{ mb} , & \text{for } 450 \text{ MeV} \leq \epsilon_r \end{cases} , \quad (24)$$

and

$$K_{p\gamma}(\epsilon_r) = \begin{cases} 0.2 , & \text{for } 150 \text{ MeV} \leq \epsilon_r < 220 \text{ MeV} \\ 0.2 , & \text{for } 220 \text{ MeV} \leq \epsilon_r < 450 \text{ MeV} \\ 0.5 , & \text{for } 450 \text{ MeV} \leq \epsilon_r \end{cases} \quad (25)$$

for the proton inelasticity. With increasing ϵ_r , the three regions that this approximation corresponds to are 1) direct pion production at threshold, 2) the enhanced cross-section at the Δ -resonance, and 3) multi-pion production in the diffractive scattering regime where photon coupling to the vector mesons ρ_0 and ω dominate. In comparison with the attenuation calculations of Mücke et al. (109) and Stanev et al. (66), we agree to ≈ 2 (4)% at $E_p = 10^{20}(10^{21})$ eV.

The electron-pair production threshold is reached when the CMBR photon-proton center-of-momentum energy $\sqrt{s} \geq 2m_e$. The CMBR spectrum peaks near the photon energy $E_{\text{CMBR}} \sim 2.35 \times 10^{-10}$ MeV. The proton Lorentz factor where electron-pair production is important is $\gamma_p \sim (1 \text{ MeV}/2.35 \times 10^{-10} \text{ MeV}) \sim 4.3 \times 10^9$, that is, for proton energies $E_p \sim 4 \times 10^{18}$ eV. The proton inelasticity per pair-production interaction is small, with $K_{p\gamma}(\epsilon_r) \simeq 2m_e < \gamma_{\text{CoM}} > / m_p \gamma \simeq 10^{-3}$. The differential cross-section peaks when the electron-pair is produced in the center-of-momentum frame, boosted by $\langle \gamma_{\text{com}} \rangle$ in the lab-frame. Our detailed calculation of the pair-production energy loss follows the treatment of Chodorowski et al. (108). The greatest photopair energy-loss rate is found at $E_p \simeq 3 \times 10^{19}$ eV when $z = 0$, and pair-production dominates other energy losses over the range $2 \times 10^{18} \text{ eV} \lesssim E_p \lesssim 6 \times 10^{19} \text{ eV}$.

In Fig. 7 we plot the attenuation lengths $X_{\text{loss}} = cdt/d \ln E$ calculated at $z = 0$ for each energy-loss process. The mean-free-path for photo-pion production is also shown.

4.2 UHECR Flux from GRBs

The UHECR flux observed on Earth results from a superposition of GRB sources distributed throughout the Universe. Our treatment of the flux cal-

culation follows the formalism of Berezhinsky and Grigor'eva (25) for diffuse spectra. The flux from a volume element $dV(z) = R^3(z)r^2dr^2d\Omega$ observed at Earth is

$$dJ(E)dE = \frac{n(z)dV(z)F(E^*, E_{max})dE^*}{(1+z)4\pi R_0^2 r^2}. \quad (26)$$

where $n(z)$ is the comoving source density, $F(E, E_{max})$ is the number of CRs produced per unit energy per unit time for an injection spectrum with power-law index p and exponential cutoff energy E_{max} , the Hubble length $R_0 = 4286$ Mpc, and E^* is the proton energy at generation which is subsequently measured with an energy $E < E^*$. To calculate a superposition of all the sources, we use $R_0 = R(z)(1+z)$, $R(z)dr = cdt$, and the relation for dt/dz from eq. (22) to obtain

$$J(E) = \frac{1}{4\pi} F(E, E_{max}) \int_0^{z_{max}} dz \frac{dt}{dz} n(z) \left(\frac{E^*}{E}\right)^{-p} \left| \frac{dE^*(E, z)}{dE} \right|, \quad (27)$$

where the term $|dE^*(E, z)/dE|$ transforms the energy interval of CR protons to account for propagation and energy losses, $n(z)$ gives the cosmic evolution described in eq. (19) and Fig. 6, and we take $z_{max} = 4.0$. Results of calculating eq. (27) for several different spectra and evolution models are found in Figs. 8, 9, 10, and 11, as described in the next section.

5 Fits to the Data and Model Implications

In this section we describe our fits to the KASCADE and HiRes-I and HiRes-II Monocular data covering the energy range from $\approx 2 \times 10^{16}$ eV to 3×10^{20} eV. The low energy portion of this range is fit with galactic CRs from GRBs (Section 3), while the high energy portion is fit by a superposition of extragalactic GRB sources (Section 4). The region where the combined flux changes from halo-dominated to extragalactic-dominated is near E_{max}^{halo} . We calculate the least- χ^2 fits for CR injection with high-energy cutoffs $E_{max} = 10^{20}$ and 10^{21} eV, and spectral indices $p = 2.2$ and 2.0 . In each case our minimum- χ^2 routine fits the halo and extragalactic normalizations and finds the best-fit value for E_{max}^{halo} . The value of E_{max}^{halo} in turn fixes parameters in the halo propagation model.

We conclude this section with model fits to the highest nine energy bins in the AGASA data covering the range 3×10^{19} eV to 3×10^{20} eV. As the AGASA results imply the possibility of a super-GZK flux, we study the quality of fits with hard spectra $p < 2.0$ from evolving GRB sources with $E_{max} = 10^{21}$ eV.

5.1 KASCADE and HiRes Data Fits

Our model has four parameters: 1) the maximum cutoff energy E_{\max} from acceleration in the GRB's relativistic shocks ($E_{\max} \gtrsim 10^{20}$ eV in order to produce an observable flux at $E > 10^{20}$ eV, in accordance with data); 2) the CR halo-component cutoff energy E_{\max}^{halo} (which is related to the spectrum and geometry of magnetic turbulence in the Galaxy); 3) the local CR luminosity density of extragalactic GRBs, assuming that GRBs follow a SFR history bounded by the curves shown in Fig. 6; and 4) the relative intensity of the galactic halo CR component to the extragalactic component. We also consider two values of the minimum energy $E_{\min} = 10^9$ eV and 10^{14} eV for CR injection, which yield identical fits but affect the overall CR energy requirements of a typical GRB. For a soft $p = 2.2$ spectrum, the baryon loading f_{CR} is a factor $\approx (10^{14}/10^9)^{0.2} = 10$ lower for the $E_{\min} = 10^{14}$ eV case than the $E_{\min} = 10^9$ eV case. Thus, with each model fit we give two values of $\dot{\epsilon}_{44}$ corresponding to $E_{\min} = 10^9$ eV and 10^{14} eV.

In total, we fit 43 data points covering the highest 4 decades of CR energies. We estimate the quality of our fits with

$$\chi^2(\vec{\alpha}) = \sum_{i=1}^{43} \left[\frac{J(E_i, \vec{\alpha}) - y_i}{\sigma_i} \right]^2 \quad (28)$$

where the y_i are data points with errors σ_i , the calculated flux is $J(E_i, \vec{\alpha})$ evaluated in energy bins E_i for an $\vec{\alpha}$ that spans the space of model parameters. The estimated best fit is the global minimum of eq. (28) found at the point $\vec{\alpha}'$ satisfying

$$\left. \frac{\partial \chi^2}{\partial \vec{\alpha}} \right|_{\vec{\alpha}'} = 0 \quad . \quad (29)$$

The reduced-minimum- χ^2 is simply $\chi_r^2 = \chi^2(\vec{\alpha}')/39$ for 39 degrees of freedom, and is reported for each case studied.

The best fit to our model places the transition region between the halo and extragalactic components in the range $\sim 2 \times 10^{17}$ eV – 2×10^{18} eV. Thus, our data set must extend to low-enough energies to make an accurate determination of E_{\max}^{halo} practicable. The lower energy data we fit is from the KASCADE all-particle spectrum (12), starting at $10^{16.35}$ eV and continuing to $10^{17.15}$ eV. The HiRes-II Monocular data set begins at $10^{17.25}$ eV and extends to $10^{19.60}$ eV, while the HiRes-I Monocular data covers the highest energies, beginning at $10^{18.55}$ eV and continuing to $10^{20.10}$ eV. Once we determine our best fitting model at the highest energies, we are then able to make predictions for halo

CRs. In Section 3.3, our best-fitting model (marked with an asterisk in Table 2) was considered in the context of the full KASCADE data set down to energies of $\lesssim 10^{15}$ eV.

To study the interplay between our model and features in the data, we fit the data with a total of 16 different sets of model parameters, as shown in Figs. 8 – 10, with the results listed in Table 2. The steepening in the data near $10^{17.6}$ eV at the second knee is a feature which rules out models with $p = 2.0$ injection. This conclusion assumes that the intercalibration between the KASCADE and HiRes data is accurate, and could be modified if reanalysis of the HECR data reveal calibration uncertainties. The extragalactic flux for $p = 2.0$ spectra fall well below the data at $E_{CR} < 10^{18}$ eV for any realistic SFR history, leaving the halo component incapable of fitting the data both above and below the second knee. Our best fitting set of model parameters is with a $p = 2.2$ injection index, $E_{max} = 10^{20}$ eV, and with the upper SFR history. This case provides the best fit to measurements of the extragalactic flux (from $\approx 2 \times 10^{17}$ eV and above), and puts the transition between galactic and extragalactic CRs in the vicinity of the second knee, consistent with evidence for a heavy-to-light composition change in this energy range (90). The ankle energy (at $\approx 3 \times 10^{18}$ eV) has a simple interpretation in our model, as a suppression of the UHECR flux from the photo-pair process (analogous to the GZK suppression from photo-pion production).

The extragalactic contribution to the CR flux in the $10^{17.6}$ eV – $10^{18.6}$ eV range is driven by the strength of the SFR evolution. The flux below $10^{18.6}$ eV is markedly higher in the upper SFR case because the UHECRs produced at redshift z are readily swept down to $\sim 10^{18}/(1+z)$ eV by propagation effects (Section 4.1). A similar result was obtained (102; 103) in the case when the cosmic evolution of GRB sources changes $\propto (1+z)^4$, which approximates the upper SFR to $z \sim 2$, but then diverges from the upper bound to the SFR derived in Ref. (94), hence predicting too high a flux at $E_{CR} < 10^{18}$ eV.

5.2 AGASA Data Fits

We study fits to the AGASA data at the highest energies $E > 3 \times 10^{19}$ eV where there are nine energy bins. The reported AGASA flux above 10^{20} eV provides a clue that UHECRs may, in fact, violate the GZK-cutoff. We explore this possibility within the context of an astrophysical source with a hard ($p < 2.0$) spectrum and cutoff $E_{max} = 10^{21}$ eV sufficient to produce a super-GZK flux. The results of five models are presented in Figure 11. For hard CR-spectra GRB sources, the CR energetics are not a problem because the high-energy portion of the spectrum receives most of the nonthermal CR energy. However, it is clear from our fits that if a super-GZK flux is verified by observations

Table 2

The results of various model fits to the KASADE, HiRes-I and HiRes-II Monocular data. The parameters p and E_{max} give the injection index and maximum injection energy of CRs from extragalactic GRBs, respectively, for the upper and lower SFR curves given in Fig. 6. The high-energy cutoff of the halo component E_{max}^{halo} and the required local cosmic ray luminosity densities f_{CR} are derived by minimizing χ_r^2 , for low-energy CR injection cutoff $E_{min} = 10^9(10^{14})$ eV. The best fit model is marked with an asterisk.

Spectrum, p	$E_{max}(\text{eV})$	SFR evol.	$E_{max}^{halo}(\text{eV})$	χ_r^2	f_{CR}
2.2	10^{20}	lower	$10^{17.48}$	1.28	821(77.5)
2.2	10^{21}	lower	$10^{17.58}$	3.10	677(65.3)
2.2*	10^{20}	upper	$10^{17.07}$	1.03	746(70.3)
2.2	10^{21}	upper	$10^{17.33}$	2.64	617(59.5)
2.0	10^{20}	lower	$10^{17.68}$	2.77	38.9(21.2)
2.0	10^{21}	lower	$10^{18.55}$	3.57	21.0(12.2)
2.0	10^{20}	upper	$10^{17.58}$	2.45	35.2(19.2)
2.0	10^{21}	upper	$10^{18.60}$	3.58	18.6(10.9)

with the Auger Observatory, it calls for either a multi-component model of astrophysical sources (including nearby sources) or new physics in the form of top-down (for recent reviews, see Refs. (110; 111)) or hybrid (for some examples, see Refs. (112; 113; 114)) scenarios.

6 High-Energy Neutrinos from Gamma-Ray Bursts

The prediction of our model that the energy output in relativistic protons and nuclei accelerated by relativistic shocks of GRBs can be much larger than the total power inferred from the observed X-ray/MeV radiation, $f_{CR} \gg 1$, suggests a very important conclusion concerning the question of detectability of GRBs by forthcoming km-scale neutrino detectors like IceCube.

A recent study (35) of this question shows that, at best, only from the brightest fraction of GRBs with neutrino fluence $\Phi_{\nu,tot}$ in the prompt phase exceeding 10^{-4} erg cm $^{-2}$, would it be possible to detect multi-TeV neutrinos by IceCube. This is a general model-independent result which only assumes that the radiation fluence derived from the X-ray/MeV γ -ray measurements in the prompt phase of GRBs does not strongly underestimate the total radiation output of GRBs (that could be missed at higher energies). This result follows from the

direct calculation of the number of muon neutrinos N_ν to be expected for a detector like IceCube, with an area $A_d = 10^{10} A_{10} \text{ cm}^2$, assuming a spectral fluence of the neutrinos $\epsilon \Phi_\nu(\epsilon) = 10^{-4} \Phi_{-4} \text{ erg cm}^{-2}$. For a spectrum of $\epsilon \Phi_\nu(\epsilon)$ with the spectral index $\simeq 0$ (i.e., with index $p_\nu \simeq 2$ for the differential number fluence $\phi_\nu(\epsilon)$), a simple derivation give $N_\nu \simeq 1.2 \Phi_{-4} A_{10} (1 + \frac{1}{2} \ln \epsilon_{14}^{-1})$ for $\epsilon_{14} < 1$, and $N_\nu \simeq 1.2 \Phi_{-4} A_{10} / \sqrt{\epsilon_{14}}$ for $\epsilon_{14} > 1$ (see (35)). Thus if the neutrino fluence is comparable to the X/ γ photon fluence, detection of ν_μ neutrinos could be expected only from very powerful GRBs, at a fluence level $\Phi_{-4} \gg 1$.

Note that $\Phi_{-4} = 1$ corresponds to the neutrino fluence $\approx 2.3 \times 10^{-4} \text{ erg cm}^{-2}$ integrated per each decade of energy. Note also the decline in the number of neutrinos to be expected per equal energy fluences per decade when $\epsilon_{14} \geq 1$. This is explained by the change in the detection efficiency $P_{\nu\mu}$ of upward-going muon neutrinos at this energy (see (115)), which can be approximated as $P_{\nu\mu} \cong 10^{-4} \epsilon_{14}^\chi$, where $\chi = 1$ for $\epsilon_{14} < 1$, and $\chi = 0.5$ for $\epsilon_{14} > 1$. Therefore, since a typical spectrum of neutrinos expected from GRBs due to photomeson interactions of HECRs extends well beyond 100 TeV, detection of even a single neutrino at multi-TeV energies would become likely only if the total fluence in the ν_μ would significantly exceed $10^{-4} \text{ erg cm}^{-2}$.

Meanwhile, the total amount of energy released in the neutrinos (including ν_e) is only about 40-50 % of the energy of secondaries resulting from photomeson interactions. Therefore at least the same amount of energy is released in the gamma-rays and electrons of multi-TeV energies produced in the secondary pion decays. For a blastwave Lorentz factor $\Gamma \sim 100\text{-}300$, the GRB radiation fields in the prompt phase are typically optically thick to photo-absorption for gamma-rays with energies above the GeV domain as is apparent from the curves in Fig. 12. Even if one assumes that the radiation in the prompt phase of a GRB is contributed only by several individual spikes, with a characteristic duration as large as $t_{spk} \sim 5\text{-}10 \text{ s}$, the source becomes transparent to gamma-rays below the GeV domain only in case of a collapsar GRB with Doppler-factor $\delta \gtrsim 300$. Therefore most of the energy injected in multi-TeV gamma-rays will be efficiently converted to hard radiation in the X-ray to sub-GeV gamma-ray domains through the synchro-Compton photon-pair cascade developing in the relativistic shock/GRB source.

Our knowledge of high-energy ($\gtrsim 100 \text{ MeV}$) emission from GRBs is limited to 7 GRBs detected with the spark chamber on EGRET (116) and the Milagro detection of GRB 970417a (117). The average spectrum of four GRBs detected simultaneously with BATSE and the EGRET spark chamber from $\lesssim 100 \text{ MeV}$ to $\approx 10 \text{ GeV}$ is consistent with a -2 photon number spectrum, implying that in these cases the $\gtrsim 100 \text{ MeV}$ fluence does not exceed the BATSE fluence by more than a factor of a few. However, the examples of the prompt and delayed high-energy emission from GRB 940217 (118), the anomalous hard component detected with BATSE and the EGRET TASC from GRB 941017 (119), and

GRB 970417a, which required ≈ 10 times more energy in the TeV range than in the BATSE range, show that the high-energy behavior of GRBs is yet poorly measured and even more poorly understood. The baseline assumption made here is to require that the energy fluence in neutrinos not exceed the fluence observed in electromagnetic radiation at hard X-ray and soft γ -ray energies.

Calculations of the neutrino fluxes expected from GRBs in case of baryon-loading factor $f_{CR} \sim 1$, i.e., assuming equal energies for relativistic hadrons and directly accelerated electrons (which are assumed to produce the observed radiation), show that even in the case of very powerful bursts with radiation fluence at the level $\Phi_{rad} \sim 10^{-4}$ ergs cm $^{-2}$, which happen only few/several times per year, the probability of detection of neutrinos by a km-scale detector would remain hopelessly small in the framework of the collapsar model unless the Doppler factor $\delta \lesssim 200$ or the variability time scale $t_{var} \ll 1$ s. A significant contribution to the target photon field density from a radiation component external to the GRB source/blob, as in the plerionic emission in the “supranova” scenario (22), or from radiation scattered by the progenitor material in the circumburst environment in the collapsar model, improves chances to detect neutrinos from GRBs (see Ref. (35) for details). This is because for large Doppler factors and $\Phi_{rad} \lesssim 10^{-4}$ ergs cm $^{-2}$, only a small fraction of the injected proton energy can be converted into secondaries through photomeson interactions of HECRs with internal photons.

The current model for the origin of galactic high and ultra-high energy CRs from GRBs requires that the nonthermal baryon loading factor $f_{CR} \gg 1$, and this prediction will be tested by the IceCube class neutrino detectors. In Fig. 13a we show the neutrino fluxes expected in the collapsar scenario from a burst at the radiation fluence level $\Phi_{rad} = 3 \times 10^{-4}$ erg cm $^{-2}$, calculated for 3 values of the Doppler factor δ assuming a GRB source at redshift $z = 1$ (for $h = 0.65$). In order to demonstrate clearly the dependence of the neutrino fluxes on δ , here we fixed the baryon-loading factor at a value $f_{CR} = 20$ for 3 values of δ . As in Fig. 12, for calculations in Fig. 13a we assume that the prompt emission is contributed by $N_{spk} = 50$ spikes with characteristic timescales $t_{spk} \simeq 1$ s each, which define the characteristic size (in the proper frame) of individual spikes through $R'_{spk} \simeq t_{spk}\delta/(1+z)$.

The numbers of (muon) neutrinos to be expected by IceCube for $\delta = 100, 200$ and 300 are $N_\nu = 1.32, 0.105$ and 0.016, respectively. We should note, however, that for the assumed value of f_{CR} , the calculated total fluence of neutrinos (both ν_μ and ν_e) produced when $\delta = 100$ is $\Phi_{\nu,tot} = 7.2 \times 10^{-4}$ erg cm $^{-2}$, i.e., by a factor $7.2/3 = 2.4$ larger than the assumed radiation fluence. It means that in the light of the arguments given above, the maximum value of the baryon loading that could be allowed if the high-energy radiation fluence is less than the X/ γ fluence for this particular case should be about 8-10, instead of 20. Consequently, the expected number of neutrinos for $\delta = 100$ should be

reduced to $\simeq 0.6$. On the other hand, in Fig. 13a the neutrino fluence for the case $\delta = 200(300)$ is equal to $\Phi_{\nu,tot} = 1.4 \times 10^{-4}(3 \times 10^{-5}) \text{ erg cm}^{-2}$, so this accommodates a baryon-loading increased from 20 up to $f_{CR} \simeq 45(200)$, with the expected number of neutrinos observed by IceCube $N_{\nu,corr} \simeq 0.23(0.16)$. If the radiation fluence at MeV – GeV energies is allowed to exceed the X/ γ fluence by an order of magnitude, a possibility that GLAST will resolve, then the expected number of detected neutrinos could be increased correspondingly.

In order to understand the degree of stability of the predicted numbers of neutrinos against the model assumptions, and most importantly with respect to the assumed number of spikes which determine the characteristic size/compactness of individual “contributing blobs,” in Fig. 13b we present the results of calculations of the ν_μ fluxes assuming $N_{spk} = 10$, corresponding to $t_{spk} \simeq 5 \text{ s}$. In this case we chose a higher $f_{CR} = 40$, anticipating a lower than previously considered fraction of energy extraction from the relativistic protons. The heavy solid and dashed curves show in Fig. 13b show the fluxes calculated for $\delta = 100$ and 300, respectively, in the collapsar scenario. The corresponding total neutrino fluences are equal to 6.9×10^{-4} and $1.3 \times 10^{-5} \text{ erg cm}^{-2}$, and the relevant numbers of ν_μ to be expected for IceCube are $N_\nu = 0.94$ and 6.4×10^{-3} . Correcting these numbers for the maximum acceptable level of neutrino fluence assuming $\Phi_{\nu,tot} \lesssim \Phi_{rad}$, results in $N_{\nu,corr} \simeq 0.4$ and 0.15 for $\delta = 100$ and 300, respectively, which are indeed close to the numbers derived above in Fig. 13a. Note that for the latter case, the implied baryon-loading factor would be as high as $f_{CR} \simeq 900$, which could still be marginally acceptable, as discussed in Section 5.1 above.

The two thin lines in Fig. 13b are calculated in the framework of a “supranova” scenario for the same values of $\delta = 100$ and 300, assuming an external radiation field density in the “plerionic nebula” with age $t_{sd} = 0.3 \text{ yr}$ (see Ref. (35) for details of calculations). The number of neutrinos to be expected when $\delta = 100$ would be practically the same as for the collapsar model, with $N_{\nu,corr} \simeq 0.5$. It is noteworthy, however, that for $\delta = 300$, the predicted probability of neutrino detection would be greatly increased relative to the collapsar model prediction, namely $N_{\nu,corr} \simeq 0.24$, which would at the same time demand a significantly smaller value for the baryon-loading factor, with $f_{CR} \simeq 15$ only.

Although these numbers are still smaller than 1, these calculations leave a non-negligible probability for detection of 1 – 2, and hopefully up to a few, neutrinos from some of most powerful GRBs during a reasonable observation time even in the case of a “collapsar” GRB with $\delta = 300$. Note that these neutrinos would be mostly at energies $> 100 \text{ TeV}$ where almost no background neutrinos are to be expected from a given direction to any single GRB (35). Such a detection would be a confirmation of high baryon-loading in GRB blast waves, and would also suggest a very significant contribution of the accelerated hadrons in the observed hard radiation through secondaries produced in the

photomeson interactions.

Another prediction of a hadronically dominated GRB model is the possible detection of gamma-rays in the multi-GeV energy domain by GLAST at a stage near the prompt phase when the density of radiation fields would still be sufficient for extraction of a small fraction of the energy of accelerated protons, but when the secondary gamma-rays would not be suppressed by the photo-absorption process. In case of relatively close GRBs, with $z \ll 1$, these gamma-rays could then be detectable also by ground-based gamma-ray detectors like VERITAS and HESS with energy thresholds ~ 100 GeV.

7 Discussion

We have proposed a model where HECRs originate from GRBs. The CR flux near the knee is assumed to result from CRs produced by a single GRB which has occurred relatively recently and not very far from us in the Milky Way. These CRs propagate diffusively in the Galactic disk and halo. The simple diffusive propagation model developed in Section 3 implies that the measured CR flux results from the modification of the injection spectrum of an impulsive CR source due to transport through a magnetic field with a given turbulence spectrum. Using a turbulence spectrum that is steeper at smaller wavenumbers and hardens at larger wavenumbers, we have fit the 2001 KASCADE data for CR ion spectra between ≈ 1 and 100 PeV, and explained the change in the all-particle spectra from $p = 2.7$ to $p \cong 3.0$. A GRB releasing $\approx 10^{52}$ ergs in HECRs, located ≈ 500 pc away, and occurring $\approx 2 \times 10^5$ years ago, provides reasonable fits to the KASCADE data.

Our model of a single GRB source making CRs at energies through the knee of the CR spectrum bears some similarity to the single-source model proposed by Erlykin and Wolfendale (120) to fit data near the knee. These authors argue, however, that propagation (“Galactic modulation”) effects cannot explain the constant rigidity break of the CR ionic species, whereas we employ a propagation model to produce that break. In this respect our propagation model treats rigidity-dependent transport as in the model of Swordy (85) and builds upon the detailed study of Atoyan, Aharonian, and Völk (82) for the spectral modification effects due to energy-dependent diffusive propagation of CRs from a single source. Our model explains, moreover, CR data not only through the first and second knees but also at the highest energies.

The turbulence spectrum that fits the CR spectrum near the knee employs a Kraichnan spectrum at small wavenumbers and a Kolmogorov spectrum at large wavenumbers. Turbulence is thought to be generated at the smallest wavenumbers or largest size scales, with subsequent energy cascading to

smaller size scales (121). It is interesting to note that there are two crucial length scales in our turbulence spectrum, namely $k_0^{-1} \approx 100$ pc, and $k_1^{-1} \approx 1$ pc. The generation of turbulence in the disk and halo of the galaxy at the larger size scale could be associated with halo-disk interactions (e.g., through the interactions of high-velocity clouds with the Galactic disk), which would deposit turbulence throughout the disk and the halo of the Galaxy on a size scale $h_d \approx 100$ pc. The smaller length scale is typical of the Sedov length scale for supernova explosions in the disk of the Galaxy. Indeed, SNe would generate a large amount of turbulence energy which could make a distinct contribution to the turbulence spectrum in this wavenumber range.

The origin of the different indices of the two components of the MHD turbulence spectra at small and large wavenumbers could be related to the time available for the turbulence energy injected at the different size scales to cascade to larger wavenumbers. Medium-energy CRs with energies between $10^9 - 10^{14}$ eV/nuc will diffuse by gyroresonant pitch-angle scattering in response to MHD waves with $k \gg 10/\text{pc}$. The model turbulence spectrum at large values of k is given by a Kolmogorov spectrum with index $q = 5/3$, as seen in Fig. (1). Because medium-energy CRs are thought to arise from a superposition of many SNe, we can treat their transport in the framework of continuous injection. As noted previously, the measured index of CRs from continuous sources is steepened by a factor $2 - q = 1/3$. If medium-energy CRs, whose measured number intensity index is ≈ 2.7 (122), result from many SNe that produce CRs which diffuse through pitch-angle scattering in a spectrum of MHD turbulence with index $q = 5/3$, then it is necessary that the injection indices of these medium-energy CRs lie between ≈ 2.3 and 2.4 .

This is a surprising result, because it is generally thought that the strong shocks in SNe accelerate and inject CRs with an injection closer to 2.0 than 2.4 (125). Such a soft injection spectrum could be avoided if medium-energy CRs diffuse in a turbulence spectrum with index $q = 3/2$. In this case, the measured index is steepened by 0.5 units compared to the injection index. If the large- k component with the steeper index is superposed on the extrapolation of the small- k component to large wavenumbers, then at sufficiently large values of k , the turbulence spectrum will change from a Kolmogorov to a Kraichnan spectrum, as illustrated by the long-dashed line in Fig. 1. In this case, a continuous injection scenario implies that an injection index of 2.2 yields an observed CR spectrum with a 2.7 number index. A $p = 2.2$ injection index is in accord with expectations from nonrelativistic shock acceleration. Note that wavenumbers of 10^3 pc^{-1} are gyroresonant with ~ 30 TeV CR protons.

An important feature of recent GRB studies is their association with SNe. CR acceleration at SN or GRB shocks is crucial for the production of CRs from the lowest energies, \lesssim GeV/nuc, to the highest energies $\gtrsim 10^{20}$ eV. The different speeds of the SN shocks in the different types of SNe ejecta

ranging from relatively slow Type II ($\approx 3000 - 10000 \text{ km s}^{-1}$) to marginally relativistic Type Ib/c is important to produce the full cosmic ray spectrum (38; 123; 124). We therefore predict that the HESS and VERITAS, with their improved sensitivity and imaging, will detect γ -ray emission from supernova remnants at a low level unless that SN has also hosted a GRB.

At energies $E \gtrsim E_{max}^{halo} \approx \text{few} \times 10^{17} \text{ eV}$, CRs stream out of galaxies to form the metagalactic CR component. We assume that GRBs evolve with cosmic epoch according to the SFR history of the universe, so that most of the UHECRs are produced at redshift $z \gtrsim 1$ when the SFR is greatest. The UHECRs have their spectrum attenuated by photo-pion, photo-pair, as well as adiabatic energy losses which become important for particle energies below $2 \times 10^{18}/(1+z) \text{ eV}$. Our best fit was found to have spectral index $p = 2.2$ and $E_{max} = 10^{20} \text{ eV}$. For these parameters, a slightly better fit was found for the stronger GRB redshift evolution (“upper SFR”). Stronger GRB evolution contributes more of the extragalactic CR flux over the range $2 \times 10^{17} \text{ eV}$ to $2 \times 10^{18} \text{ eV}$ than the lower SFR case, giving a best-fit value $E_{max}^{halo} \sim 2 \times 10^{17} \text{ eV}$. This is an effect of CR attenuation from photopion and photopair production processes where all of the CR flux produced at $E \gtrsim 2 \times 10^{18} \text{ eV}$ (and $z \gtrsim 1$) are swept to lower energies. Crucial for deriving these conclusions are the relative calibrations of the KASCADE and High-Res experiments.

Our best fit to the UHECR data gives a measure of the local GRB luminosity density $\dot{\epsilon}_{CR}$ required in CRs. We find $f_{CR} \approx 70$ for $E_{min} = 10^{14} \text{ eV}$ and $\delta = 300$. This implies that GRBs must be baryon-loaded by a factor $\gtrsim 50$ if this model for HEERs is correct. The precise value of f_{CR} varies with Doppler factor according to $f_{CR} \approx 70(300/\delta)^{0.4}$, for a $p = 2.2$ injection spectrum. Nonthermal baryon-loading factors $f_{CR} \gg 1$ implies that GRBs should also be luminous in high-energy neutrinos. In section 6 we calculate the fluence in neutrinos and predict that $\approx 0.1 - \text{few}$ neutrinos of energy 100 TeV–100 PeV may be observable in IceCube a few times per year from individual GRB explosions, which depends on the radiation fluence measured from GRBs at $\gtrsim 100 \text{ MeV} - \text{GeV}$ energies, which is not yet well known.

In a collapsar model calculation (35), the predicted number of neutrinos depends sensitively on δ , because the density of internal synchrotron photons is much larger for smaller values of δ . The X-ray flashes (68) may be “dirty fireball” GRBs, which are similar to classical long-duration GRBs, though with larger (thermal) baryon loading and smaller average values of δ (69). This suggests that the X-ray flashes may be more promising candidates for neutrino detection than GRBs with peak photon energies of the νF_ν flux at several hundred keV energies.

The low statistics of current data at the highest energies make unclear the presence or absence of a super-GZK UHECR component. The HiRes data

appears to be consistent with the GZK effect, thereby favoring an origin of UHECRs in “conventional” astrophysical sources. If the UHECR flux is found to exceed prediction of a GZK cutoff, then this could be evidence of new physics, could indicate the existence of super-GZK sources of cosmic rays within ~ 100 Mpc from Earth, or both. Our current interpretation of the data is made uncertain by results from the AGASA experiment (14) which reveals a super-GZK flux, in conflict with the HiRes and Fly’s Eye data (13) (see, however, Ref. (16), who argue that the discrepancy is not serious given the uncertainties in calibration and the statistical variance of CR fluxes measured at such high energies).

The possibility of new physics associated with a super-GZK CR flux has generated much interest. Scenarios for a super-GZK flux include the Z-burst scenario (112), magnetic monopole primaries (113; 114), and the decay of supermassive relic particles(110). (For a recent review, see Ref. (111).) Another approach to generate super-GZK fluxes is from astrophysical sources distributed within a GZK-distance from Earth, $\lesssim 140$ Mpc. The Auger detector should resolve this question by measuring ≈ 30 events per year above 10^{20} eV.

8 Conclusions

The variable, highly luminous GRB emissions, the association of the sources of GRBs with supernovae, and the availability of different modes of particle acceleration in the relativistic outflows and shocks of GRB blast waves, lead to the conclusion that GRB explosions are effective cosmic-ray accelerators. Observational evidence indicates that GRB sources are found in regions of active star formation, and that the GRB luminosity density tracks the star formation history of the universe, so that GRB sources are also found in our Galaxy.

In this paper, we have investigated the hypothesis that GRBs are the sources of HECRs. Our model provides a unified source-type to fit all of the CRs from some minimum CR energy produced in GRBs, which could be somewhere $\lesssim 10^{14}$ eV, to a maximum energy $\gtrsim 10^{20}$ eV. The total CR flux that we calculate is a superposition of CRs originating from a past GRB in our Galaxy in whose HECR halo we inhabit (with a gradual transition at lower energies to CRs contributed from ordinary SN events with sub-relativistic blast waves), and $\gtrsim 3 \times 10^{17}$ eV CRs and UHECRs originating in extragalactic GRBs and GRBs at cosmological distances. The HECR all-particle spectrum and our model fit to this data are shown in Fig. 14.

For an injection index $p = 2.2$, which gives the best fit to the UHECR data, the local luminosity density for CR injection is $\dot{\epsilon}_{CR} \approx 70 \times 10^{44}$ ergs Mpc $^{-3}$

yr^{-1} if the minimum CR injection energy is $\approx 10^{14}$ eV. A GRB model for HECR production therefore necessarily demands that GRB blast waves are hadronically dominated by nearly 2 orders of magnitude.

Such a requirement has important consequences for 100 MeV – GeV – TeV γ -ray emission and high-energy ($\gtrsim 100$ TeV) neutrino detection. Allowed hadronic production in GRB blast waves will make γ rays of comparable fluence as the neutrino fluence. Insisting that the high-energy radiation fluence from a photomeson cascade can only reach the level of the X/ γ emission measured with BATSE (unless it is missed by detectors operating at larger energies), we have shown that $\gtrsim 1$ neutrino could be detected coincident with a GRB at the fluence level $\gtrsim 3 \times 10^{-4}$ ergs cm^{-2} by IceCube.

If GLAST shows that GRBs are much more fluent at $\gtrsim 100$ MeV energies than at X/ γ energies, then in these GRBs one could expect a few high-energy neutrinos. Detection of even 1 or 2 neutrinos from GRBs with IceCube or a northern hemisphere neutrino telescope would unambiguously demonstrate the high nonthermal baryon load in GRBs. High-energy neutrino detection, especially from GRBs with bright 100 MeV – GeV emission components, or from GRBs with small Lorentz factors or large baryon-loading such as the X-ray bright GRBs, would provide compelling support for this scenario for the origin of the cosmic rays.

The work of C.D.D. is supported by the Office of Naval Research and NASA *GLAST* science investigation grant DPR # S-15634-Y. A.A. acknowledges support and hospitality during visits to the High Energy Space Environment Branch. The work of S.D.W. was performed while he held a National Research Council Research Associateship Award at the Naval Research Laboratory (Washington, D.C).

References

- [1] M. Vietri, *Astrophys. J.* 453 (1995) 883.
- [2] E. Waxman, *Phys. Rev. Letters* 75 (1995) 386.
- [3] C. D. Dermer, *Astrophys. J.* 574 (2002) 65, and astro-ph/0005440 v. 1.
- [4] S. G. Djorgovski et al., in *Gamma Ray Bursts in the Afterglow Era*, E. Costa et al., eds. (Springer: Berlin, 2001), 218.
- [5] P. Mészáros, *Ann. Rev. Astron. Astrophys.* 40 (2002) 137.
- [6] J. van Paradijs, C. Kouveliotou, and R. A. M. J. Wijers, *Ann. Rev. Astron. Astrophys.* 38 (2000) 379.
- [7] E. Pian et al., *Astrophys. J.* 536 (2000) 778.
- [8] J. Hjorth et al., *Nature* 423 (2003) 847.

- [9] G. J. Fishman, C. A. Meegan, *Ann. Rev. Astron. Astrophys.* 33 (1995) 415.
- [10] H. Ulrich et al., in: 27th International Cosmic Ray Conference (Copernicus Gesellschaft: Hamburg, Germany) 1 (2001) 97.
- [11] M. Bertaina et al., in: 27th International Cosmic Ray Conference (Copernicus Gesellschaft, Hamburg, Germany) 2 (2001) 792.
- [12] K.-H. Kampert et al., in: 27th International Cosmic Ray Conference (Copernicus Gesellschaft, Hamburg, Germany) Invited, Rapporteur, and Highlight Papers (2001) 240.
- [13] T. Abu-Zayyad et al. (2003) (astro-ph/0208243).
- [14] M. Takeda et al., *Phys. Rev. Letters* 81 (1998) 1163.
- [15] J. N. Bahcall, E. Waxman, *Phys. Lett. B* 556 (2003) 1.
- [16] D. De Marco, P. Blasi, A. V. Olinto, *Astropar. Phys.* 20 (2003) 53.
- [17] M. Nagano, A. A. Watson, *Rev. Mod. Phys.* 72 (2000) 689.
- [18] S. Razzaque, P. Mészáros, E. Waxman, *Phys. Rev. D*, in press (2003) (astro-ph/0303505).
- [19] C. D. Dermer, M. Humi, *Astrophys. J.* 536 (1999) 479.
- [20] E.V. Derishev, F.A. Aharonian, V.V. Kocharovsky, V. V. Kocharovsky, *Phys. Rev. D* 68 (2003) 043003.
- [21] Y. A. Gallant, A. Achterberg, M. Not. Roy. Astron. Soc. 305 (1999) L6.
- [22] Königl, A. & Granot, J. 2002, *Astrophys. J.*, 574, 134
- [23] M. Vietri, D. De Marco, D. Guetta, *Astrophys. J.* 592 (2003) 378.
- [24] C. T. Hill, D. N. Schramm, *Phys. Rev. D* 31 (1985) 564.
- [25] V. S. Berezinskii, S. I. Grigor'eva, *Astron. Astrophys.* 199 (1988) 1; (e) 210 (1989) 462.
- [26] A. Mücke, R. Engel, J. P. Rachen, R. J. Protheroe, T. Stanev, T. 2000, *Computer Physics Comm.* 124 (2000) 290.
- [27] J. Bednarz, M. Ostrowski, 1998, *Phys. Rev. Letters* 80 (1998) 3911.
- [28] J. G. Kirk, A. W. Guthmann, Y. A. Gallant, A. Achterberg, *Astrophys. J.* 542 (2000) 235.
- [29] Ginzburg, V. L., and Syrovatskii, S. I., *The Origin of Cosmic Rays* (New York, MacMillan, 1964).
- [30] Hayakawa, S., *Cosmic Ray Physics* (New York, Wiley, 1969).
- [31] E. Waxman, J. Bahcall, *Phys. Rev. D* 59 (1999) 23002.
- [32] M. Böttcher, C. D. Dermer, *Astrophys. J.* 529 (2000) 635, (e) 536 (2000) 513.
- [33] M. Böttcher, C. D. Dermer, *Astrophys. J.* 499 (1998) L13.
- [34] B. Zhang, and P. Mészáros *Astrophys. J.* 559 (2001) 110.
- [35] C. D. Dermer, A. Atoyan, *Phys. Rev. Letters* 91 (2003) 071102.
- [36] M. Milgrom, V. Usov, *Astropart. Phys.* 4 (1996) 365.

Section 2.

- [37] C. D. Dermer, in: *High Energy Gamma-Ray Astronomy*, F. Aharonian and H. Völk, eds. (AIP, New York, 2001) p. 202.
- [38] C. D. Dermer, in: 27th International Cosmic Ray Conference (Coperni-

- cus Gesellschaft, Hamburg, Germany) Invited, Rapporteur, and Highlight Papers (2001) 72.
- [39] P. Sommers, in: 27th International Cosmic Ray Conference (Copernicus Gesellschaft, Hamburg, Germany) Invited, Rapporteur, and Highlight Papers (2001) 170.
 - [40] J. S. Bloom et al., *Astrophys. J.* 518 (1999) L1.
 - [41] T. J. Galama, R. A. M. J. Wijers, *Astrophys. J.* 549 (2001) L209.
 - [42] D. E. Reichart, *Astrophys. J.* 521 (1999) L111.
 - [43] J. S. Bloom, et al. *Astrophys. J.* 572 (2002) L45.
 - [44] L. Amati, et al. *Science* 290 (2000) 953.
 - [45] L. Piro, et al. *Science* 290 (2000) 955.
 - [46] L. Piro, et al. *Astrophys. J.* 514 (1999) L73.
 - [47] A. Yoshida et al., *Astrophys. J.* 557 (2001) L27.
 - [48] L. A. Antonelli et al., *Astrophys. J.* 545 (2000) L39.
 - [49] J. N. Reeves et al., *Nature*, 416 (2002) 512.
 - [50] S. E. Woosley, *Astrophys. J.* 405 (1993) 273.
 - [51] M. Böttcher, C. L. Fryer, C. D. Dermer, *Astrophys. J.* 567 (2002) 441.
 - [52] M. Vietri and L. Stella, *Astrophys. J.*, 507 (1998) L45.
 - [53] C. L. Fryer, S. E. Woosley, D. Hartmann, *Astrophys. J.* 526 (1999) 152.
 - [54] R. Blandford, D. Eichler, *Phys. Rep.* 154 (1987) 1.
 - [55] R. Schlickeiser, *Astron. Astrophys.* 136 (1984) 227.
 - [56] Inoue, S., Guetta, D., & Pacini, F. 2003, *Astrophys. J.* 583 (2003), 379.
 - [57] P. Mészáros, M. J. Rees, *Astrophys. J.* 405 (1993) 278.
 - [58] T. C. Weekes, in: *High Energy Gamma-Ray Astronomy*, F. and H. Völk, eds. (AIP, New York, 2001) p. 15.
 - [59] F. A. Aharonian, et al., *Astron. Astrophys.* 370 (2001) 112.
 - [60] R. Enomoto, R. et al., *Nature* 416 (2002) 823.
 - [61] O. Reimer, M. Pohl, *Astron. Astrophys.* 390 (2002) L43.
 - [62] T. K. Gaisser, *Cosmic Rays and Particle Physics* (New York, Cambridge University Press, 1990).
 - [63] V. S. Berezhinskii, S. V. Bulanov, V. A. Dogiel, V. L. Ginzburg, V. S. Ptuskin (eds.), *The Astrophysics of Cosmic Rays* (Elsevier, New York, 1991).
 - [64] R. Schlickeiser, *Cosmic Ray Astrophysics* (Springer-Verlag, Berlin, 2002), chpts. 14 and 17.
 - [65] P. O. Lagage, C. J. Cesarsky, *Astron. Astrophys.* 118 (1983) 223.
 - [66] T. Stanev, R. Engel, A. Mücke, R. J. Protheroe, J. P. Rachen, *Phys. Rev. D* 62 (2000) 93005.
 - [67] F. W. Stecker, *Astropart. Phys.* 14 (2000) 207.
 - [68] J. Heise, J. in't Zand, R. M. Kippen, and P. M. Woods, *Gamma-ray Bursts in the Afterglow Era*, ed. by E. Costa, F. Frontera, and J. Hjorth (Berlin, Springer, 2001) 16.
 - [69] C. D. Dermer, J. Chiang, M. Böttcher, *Astrophys. J.* 513 (1999) 656.
 - [70] A. Panaitescu, P. Kumar, *Astrophys. J.* 554 (2001) 667.
 - [71] D. A. Frail et al. *Astrophys. J.* 562 (2001) L55.

- [72] R. A. M. J. Wijers, J. S. Bloom, J. S. Bagla, P. Natarajan, *Monthly Not. Roy. Astron. Soc.* 294 (1998) L13.
- [73] D. L. Band, *Astrophys. J.* 578 (2002) 806.
- [74] M. Schmidt, *Astrophys. J.* 552 (2001) 36.

Section 3.

- [75] P. L. Biermann, P. A. Strittmatter, *Astrophys. J.* 322 (1987) 643.
- [76] C. D. Dermer, J. A. Miller, H. Li, *Astrophys. J.* 456 (1996) 106.
- [77] S. Colafrancesco, P. Blasi, *Astropar. Phys.* 9 (1998) 227.
- [78] P. Goldreich, S. Sridhar, *Astrophys. J.* 485 (1997) 680.
- [79] Drury, L. O'C., *Repts. Theor. Phys.* 46 (1983) 973.
- [80] P. Blasi, *Astrophys. J.* 532 (2000) L9.
- [81] R. Z. Sagdeev, A. A. Galeev, *Nonlinear Plasma Theory* (New York, Benjamin, 1969).
- [82] A. M. Atoyan, F. A. Aharonian, H. J. Völk, *Phys. Rev. D* 52 (1995) 3265.
- [83] E. Anders, N. Grevesse, *Geochimica et Cosmochimica Acta* 53 (1989) 197.
- [84] M. Roth et al., in: 28th International Cosmic Ray Conference, Tokyo, Japan.
- [85] S. P. Swordy, 24th Int. Cosmic-Ray Conf. (Rome), 2 (1995) 697.
- [86] S. P. Swordy, J. L'Heureux, P. Meyer, and D. Müller, *Astrophys. J.* 403 (1993) 658.
- [87] V. L. Ginzburg, V. S. Ptuskin, *Rev. Mod. Phys.* 48 (1976) 161.
- [88] A. A. Watson, *Adv. Space Res.* 4 (1984) 35.
- [89] A. M. Hillas, *Ann. Rev. Astron. Astrophys.* 22 (1984) 425.

Section 4.

- [90] D. J. Bird et al., *Phys. Rev. Lett.* 71 (1993) 3401.
- [91] K. Greisen, *Phys. Rev. Lett.* 16 (1966) 748.
- [92] G. T. Zatsepin and V. A. Kuzmin, *JETP Lett.* 4 (1966) 78.
- [93] P. Madau, L. Pozzetti, and M. Dickinson, *Astrophys. J.* 498 (1998) 106.
- [94] A. W. Blain et al., *Mon. Not. R. Astron. Soc.* 309 (1999) 715.
- [95] C. Gronwall, in T. X. Thuan et al., eds., *Dwarf Galaxies and Cosmology*, Proc. XVIII Moriond Meeting (astro-ph/9806240).
- [96] M. A. Treyer et al., *Mon. Not. R. Astron. Soc.* 300 (1998) 303.
- [97] L. Tresse and S. J. Maddox, *Astrophys. J.* 459 (1998) 691.
- [98] S. J. Lilly, O. LeFevre, F. Hammer, and D. Crampton, *Astrophys. J.* 460 (1996) L1.
- [99] A. J. Connolly et al., *Astrophys. J.* 486 (1997) L11.
- [100] P. Madau et al., *Mon. Not. R. Astron. Soc.* 283 (1996) 1388.
- [101] M. Pettini et al., *Astrophys. J.* 508 (1998) 539.
- [102] S. T. Scully and F. W. Stecker, *Astropart. Phys.* 16 (2002) 271.
- [103] V. S. Berezhinskii, A. Z. Gazizov, and S. I. Grigorieva, (hep-ph/0204357).
- [104] C. L. Bennett, et al. 2003, *Astrophys. J. S.* 148, 1.
- [105] D. N. Spergel et al., *Astrophys. J. S.* 148 (2003) 175.

- [106] J. N. Tonry et al., *Astrophys. J.* 594 (2003) 1.
- [107] A. M. Atoyan and C. D. Dermer, *Astrophys. J.* 586 (2003) 79.
- [108] M. J. Chodorowski, A. A. Zdziarski, and M. Sikora, *Astrophys. J.* 400 (1992) 181.
- [109] A. Mucke, J. P. Rachen, R. Engel, R. J. Protheroe, and T. Stanev, *Pub. Astr. Soc. Australia* 16 (1999) 160.

Section 5.

- [110] M. Drees, PASCOS 03 (hep-ph/0304030).
- [111] L. Anchordoqui et al., *Int. J. Mod. Phys. A* 18 (2003) 2229.
- [112] T. J. Weiler, *Astropart. Phys.* 11 (1999) 303.
- [113] T. W. Kephart and T. J. Weiler, *Astropart. Phys.* 4 (1996) 271.
- [114] S. D. Wick, T. W. Kephart, T. J. Weiler, and P. L. Biermann, *Astropart. Phys.* 18 (2003) 663.

Section 6.

- [115] T. K. Gaisser, F. Halzen, and T. Stanev, *Phys. Repts.* 258(3) (1995) 173.
- [116] B. D. Dingus, J. R. Catelli, and E. J. Schneid, *Fourth Huntsville Symposium on Gamma Ray Bursts*, eds. C. A. Meegan, R. D. Preece, and T. M. Koshut (New York: AIP), 349.
- [117] R. Atkins, et al., *Astrophys. J.* 583 (2003) 824.
- [118] K. Hurley, et al., *Nature* 372 (1994) 652.
- [119] M. M. González, B. L. Dingus, Y. Kaneko, R. D. Preece, C. D. Dermer, and M. S. Briggs, *Nature* 424 (2003) 749.

Section 7.

- [120] A. D. Erlykin and A. W. Wolfendale, *Adv. Space Res.* 27 (2002) 803.
- [121] J. Cho, A. Lazarian, and E. T. Vishniac, *Astrophys. J.* 566 (2002) L49.
- [122] J. A. Simpson, *Ann. Rev. Astron. Astrophys.* 33 (1983) 323.
- [123] L. G. Sveshnikova, *Astron. Astrophys.* 409 (2003) 799.
- [124] E. Berger, astro-ph/0309714
- [125] J. G. Kirk, *Saas-Fee Advanced Course 24: Plasma Astrophysics* (1994) 225.

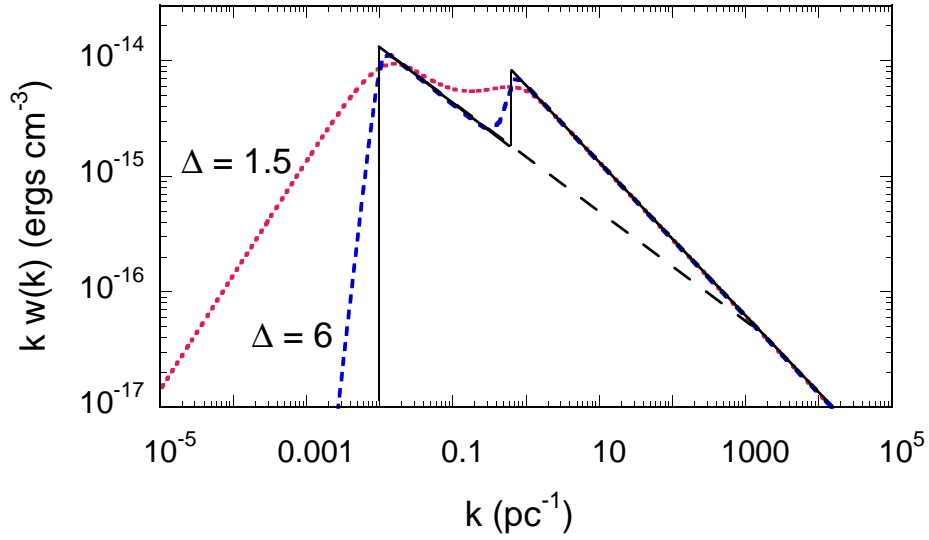


Fig. 1. Wave turbulence spectrum used to model CR propagation in the Galaxy. The mean magnetic field is assumed to be $3 \mu\text{G}$. An idealized model is shown by the solid lines and, after smoothing, by the dotted and short-dashed curves for the smoothing parameter $\Delta = 1.5$ and 6 , respectively. The parameters for the model used in the fits are $\xi = 0.1$, $f_H = 0.2$, $k_0 = 1/100 \text{ pc}^{-1}$, $k_1 = 1/1.6 \text{ pc}^{-1}$, and $\Delta = 1.5$. The extension of the small-wavenumber ($k < k_1$) turbulence spectrum intersects the large-wavenumber ($k > k_1$) spectrum at $k \approx 1000 \text{ pc}^{-1}$, as shown by the long-dashed line.

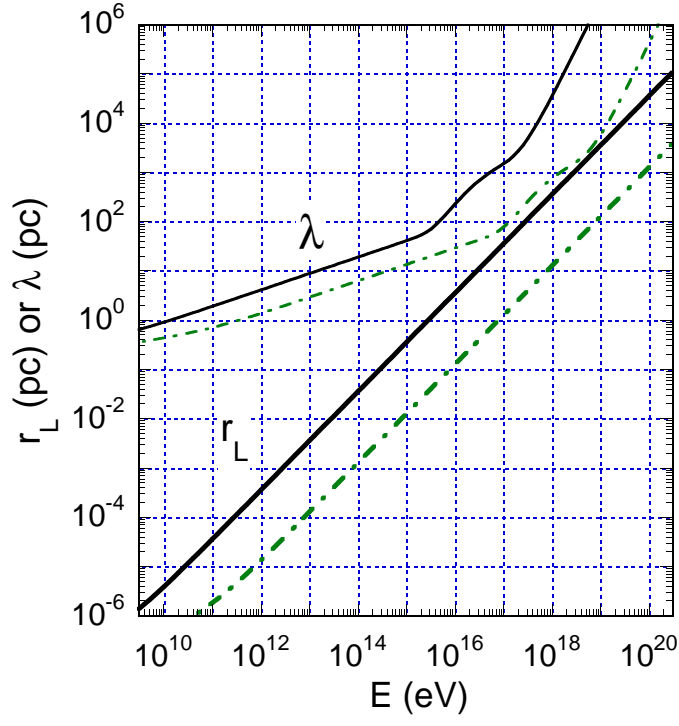


Fig. 2. Larmor radius r_L and mean-free-path λ of CR protons (solid curves) and Fe nuclei ($Z = 26, A = 56$; dot-dashed curves) with total energy E in a magnetic field with mean strength of $3 \mu\text{G}$. The wave turbulence spectrum given by Fig. 1 with $\Delta = 1.5$ is used to calculate λ .

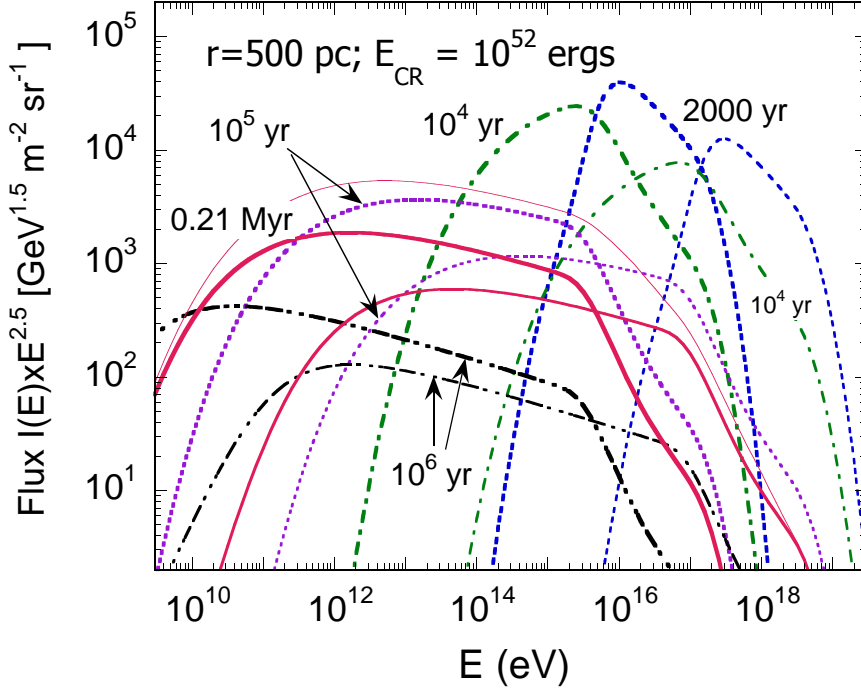


Fig. 3. Temporal evolution of the fluxes of CR protons (heavy curves) and Fe nuclei (light curves) measured by an observer 500 pc from a GRB that took place at earlier times given by the labels on the curves. The GRB was assumed to inject 10^{52} ergs total energy in cosmic rays with an ionic composition given by Table 1 and a low-energy cutoff at $(\beta\gamma)_{min} = 0.01$ (≈ 50 keV). Shown by the upper thin solid curve is the all-particle flux at time $t = 0.21$ Myr used to fit the KASCADE data. Note that the fluxes have been multiplied by $E^{2.5}$, where E is the CR particle kinetic energy.

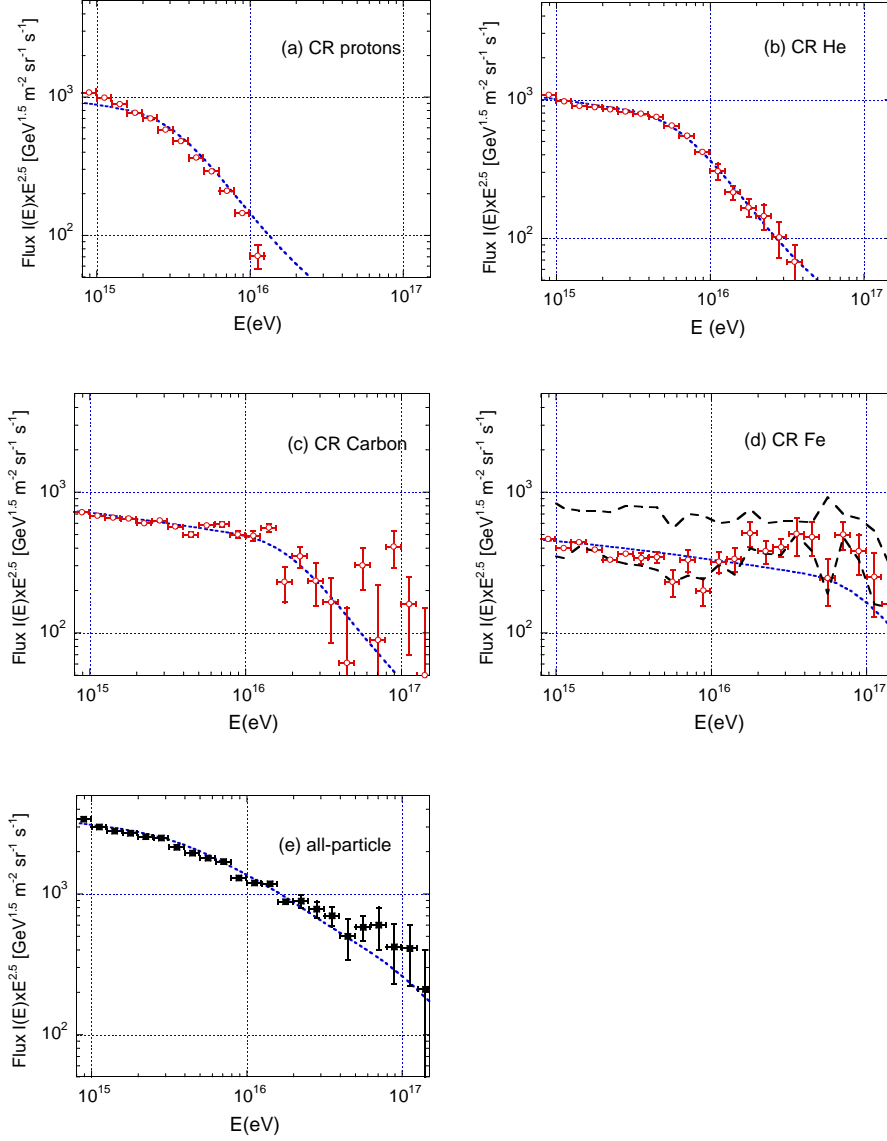


Fig. 4. Data points show preliminary KASCADE measurements of the CR proton (panel a), He (panel b), Carbon (panel c), Fe (panel d), and the all-particle spectrum (panel e), along with model fits (dotted curves) to the CR ionic fluxes. In the model, a GRB that occurred 2.1×10^5 years ago and at a distance of 500 pc injects 10^{52} ergs in CRs, with ionic compositions given in Table 1. The CRs isotropically diffuse via pitch-angle scattering with an energy-dependent mean-free-path λ in an MHD turbulence field given by Fig. 1.

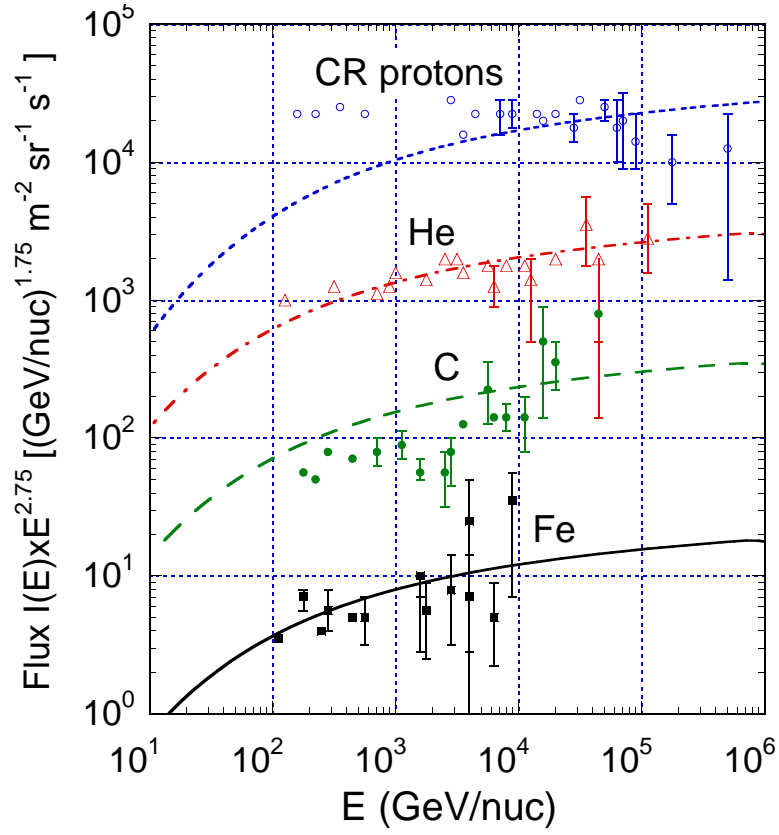


Fig. 5. Contributions to the CR flux in the GeV/nuc - TeV/nuc range for a single source with a low-energy cutoff determined by the minimum injection momentum $(\beta\gamma)_{min} = 0.01$. Data is taken from the papers by Swordy et al. (86; 85). The excess flux from the model, especially for CR Carbon, suggest a low-energy cutoff in the CR injection spectrum from GRBs.

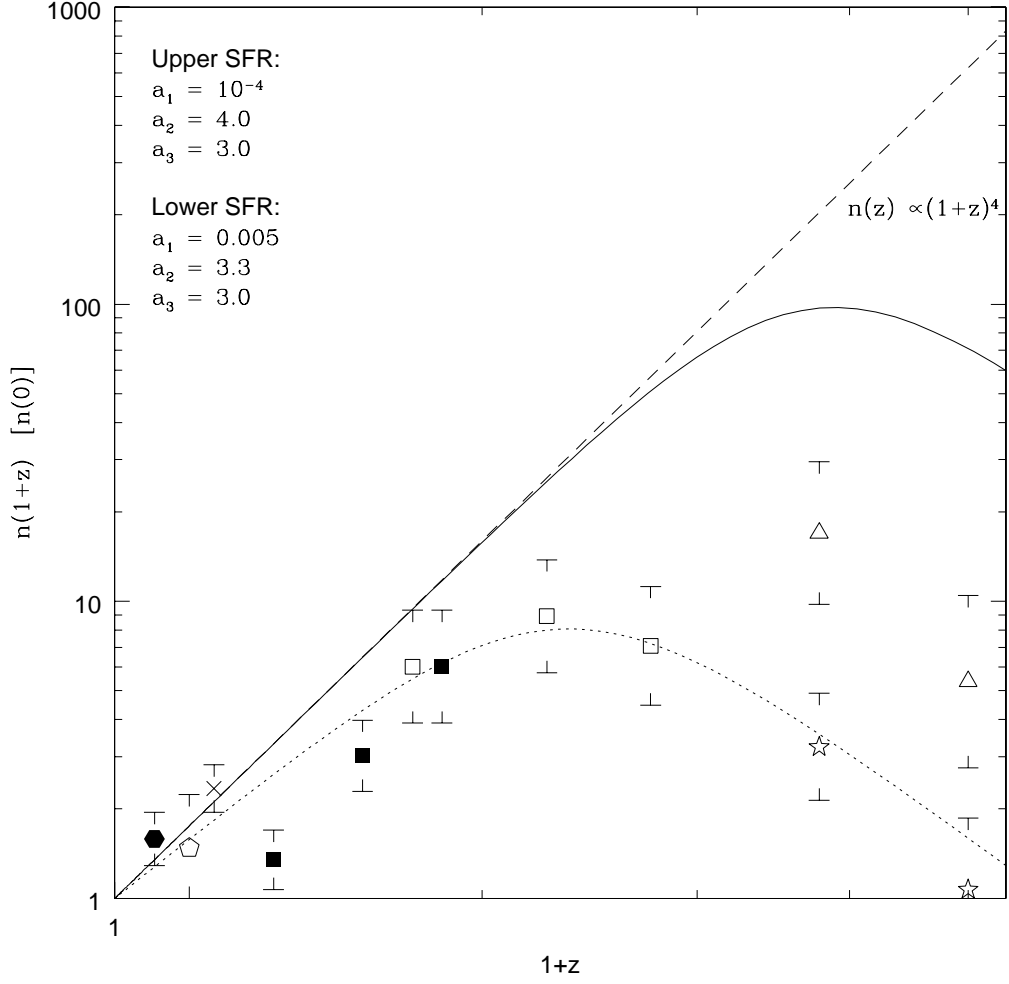


Fig. 6. The evolution of the rate density of GRBs as a function of $1+z$, shown in comparison to measurements of the star formation rate (SFR) inferred from measurements of restframe optical/UV emission from galaxies. The data, normalized with respect to a SFR of $0.09 \text{ M}_\odot \text{ Mpc}^{-3} \text{ yr}^{-1}$, are listed in order of increasing redshift and denoted for different measurements by the following symbols: filled hexagons (95), open hexagons (96), diagonal crosses (97), filled squares (98), open squares (99), and open stars (100). A SFR modification for dust extinction is given by the open triangles (101). We use the function given in eq. (19) with $a = 0.005(0.0001)$, $b = 3.3(4.0)$, and $c = 3.0(3.0)$ for each of the models tested in our UHECR calculations. The dotted curve, based upon optical/UV observations, is arguably a lower limit to the SFR evolution. An extreme correction for dust extinction (94) gives the stronger evolution shown by the middle, solid curve. For comparison, the dashed curve displays the relation $n(z) = n(0)(1+z)^4$ used by other authors (102; 103).

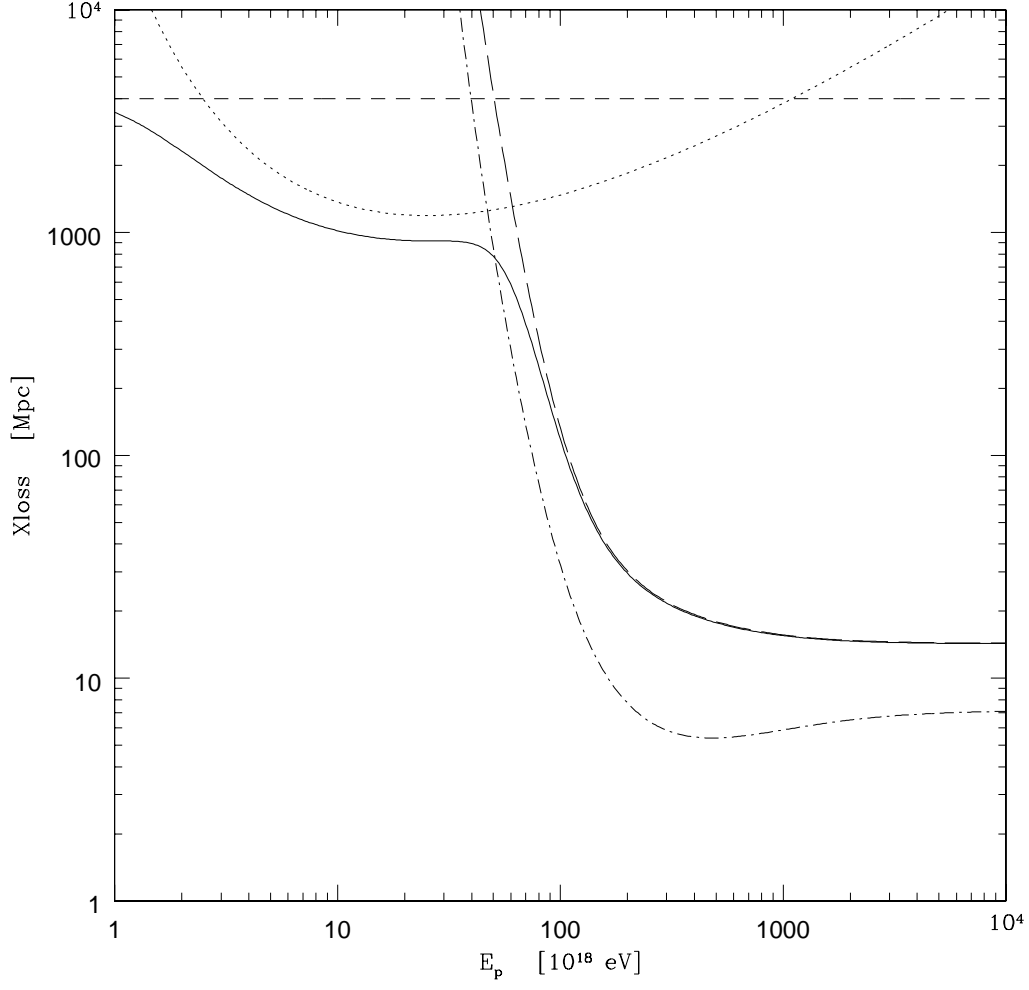


Fig. 7. The distance X_{loss} over which a proton loses a fraction e^{-1} of its energy as a function of proton energy, calculated at $z = 0$. The solid line is the total energy-loss distance from the sum of the energy-loss distances X_{loss} for electron-pair production (dotted), momentum red-shifting (short-dashed), and pion production (long-dashed). The mean-free-path for a pion production interaction is also plotted (dash-dotted).

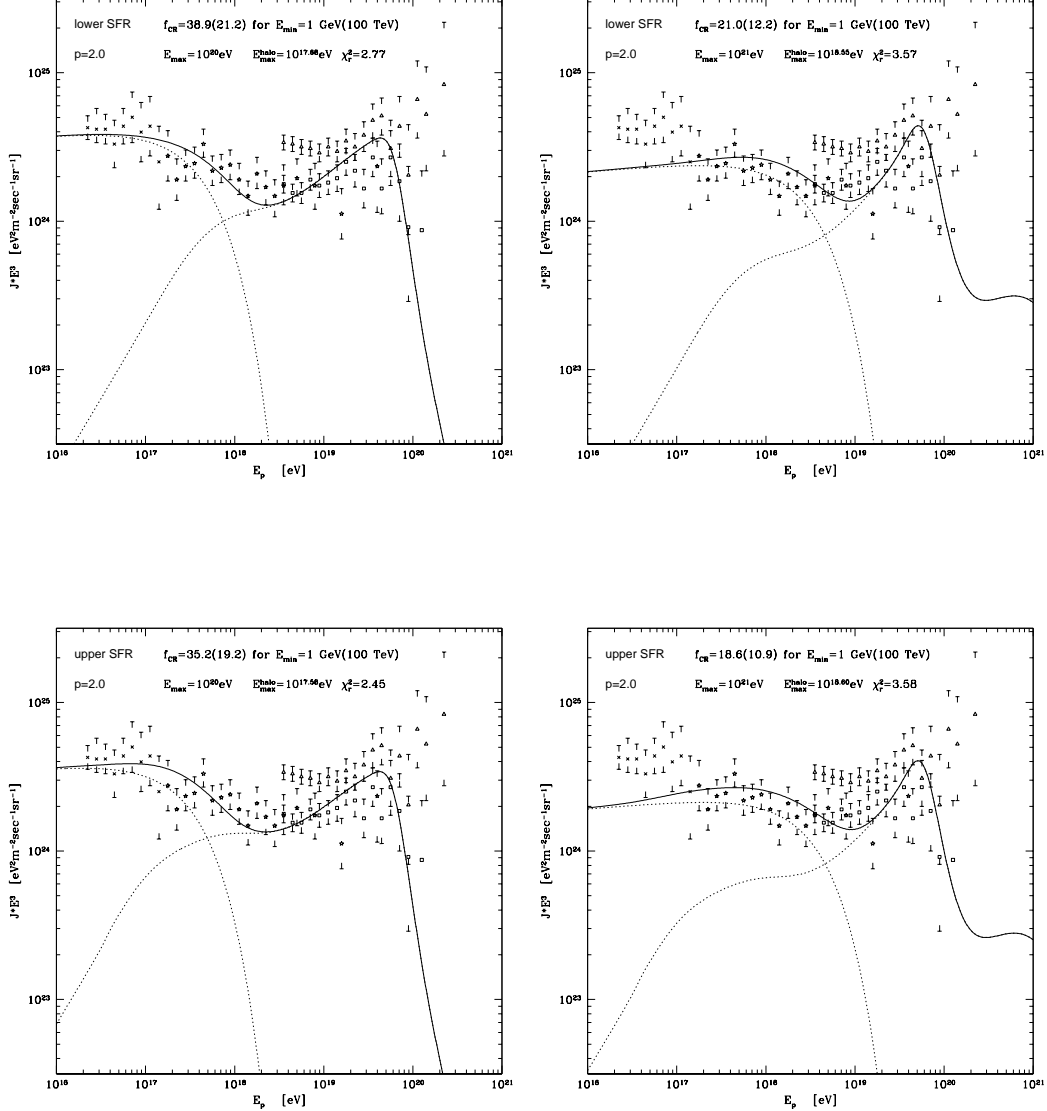


Fig. 8. Fits to UHECR data for model with injection spectral index $p = 2.0$. The fits to the KASCADE (crosses), HiRes-I Monocular (squares), HiRes-II Monocular (stars) data assume various spectral cutoffs of the source, and lower and upper SFR histories and E_{max} as labeled on the figures. Although the AGASA data (triangles) are shown, they are not included in the fits. The cutoff energies for the halo component E_{max}^{halo} , reduced χ_r^2 , and requisite local CR luminosities f_{CR} are given on each figure.

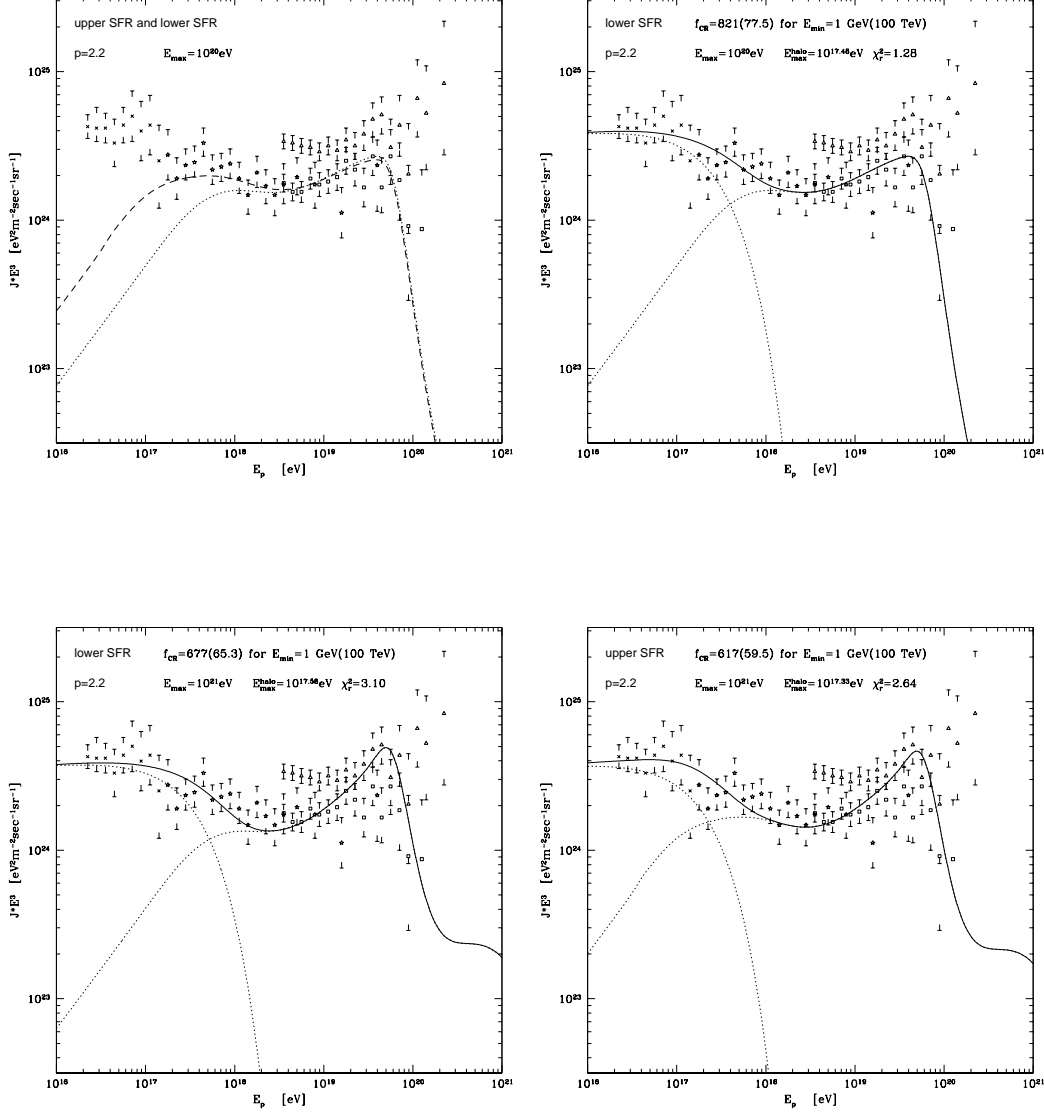


Fig. 9. Upper-left figure gives a comparison of the upper versus lower SFR evolution. Attenuation of the CR flux originating at energies $> 2 \times 10^{18}$ eV and $z > 1$ are swept by photo-pion and photo-pair processes down to lower energies. The increased number of CRs injected for the upper SFR yields a significantly larger flux of CRs in the range 2×10^{17} eV to 2×10^{18} eV. The remaining three figures are the same as in Fig. 8, except that the injection index is now $p = 2.2$.

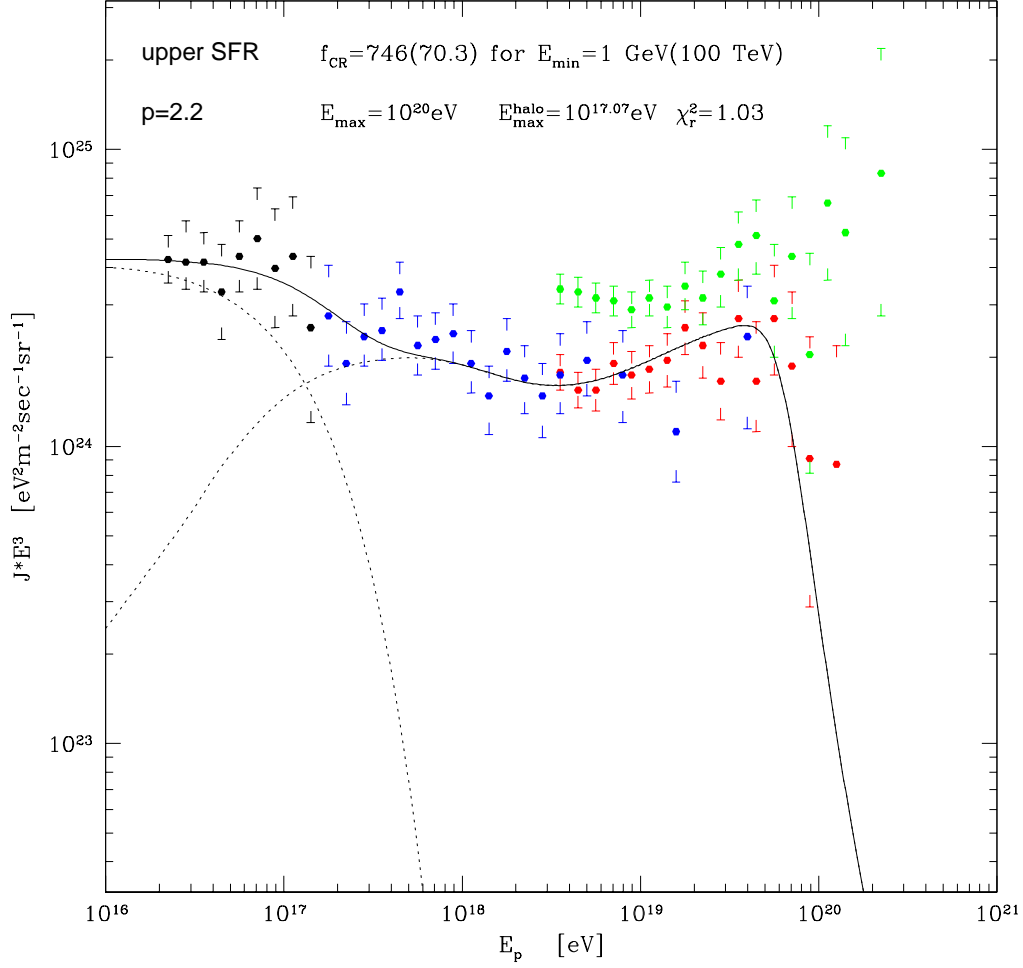


Fig. 10. Best fit to the Kascade (black points), HiRes-I Monocular (red points), HiRes-II Monocular (blue points) data assuming a spectral cutoff at the source of $E_{max} = 10^{20}$ eV and using the upper limit to the SFR evolution. We also show the AGASA data (green points) but do not include these in our fits. The cutoff energy for the halo component is $E_{max}^{halo} = 10^{17.07}$ eV giving a $\chi_r^2 = 1.03$. The requisite baryon loading factor for this fit is $f_{CR} = 746(70.3)$ for a low energy cutoff at the source of $E_{min} = 10^9(10^{14})$ eV.

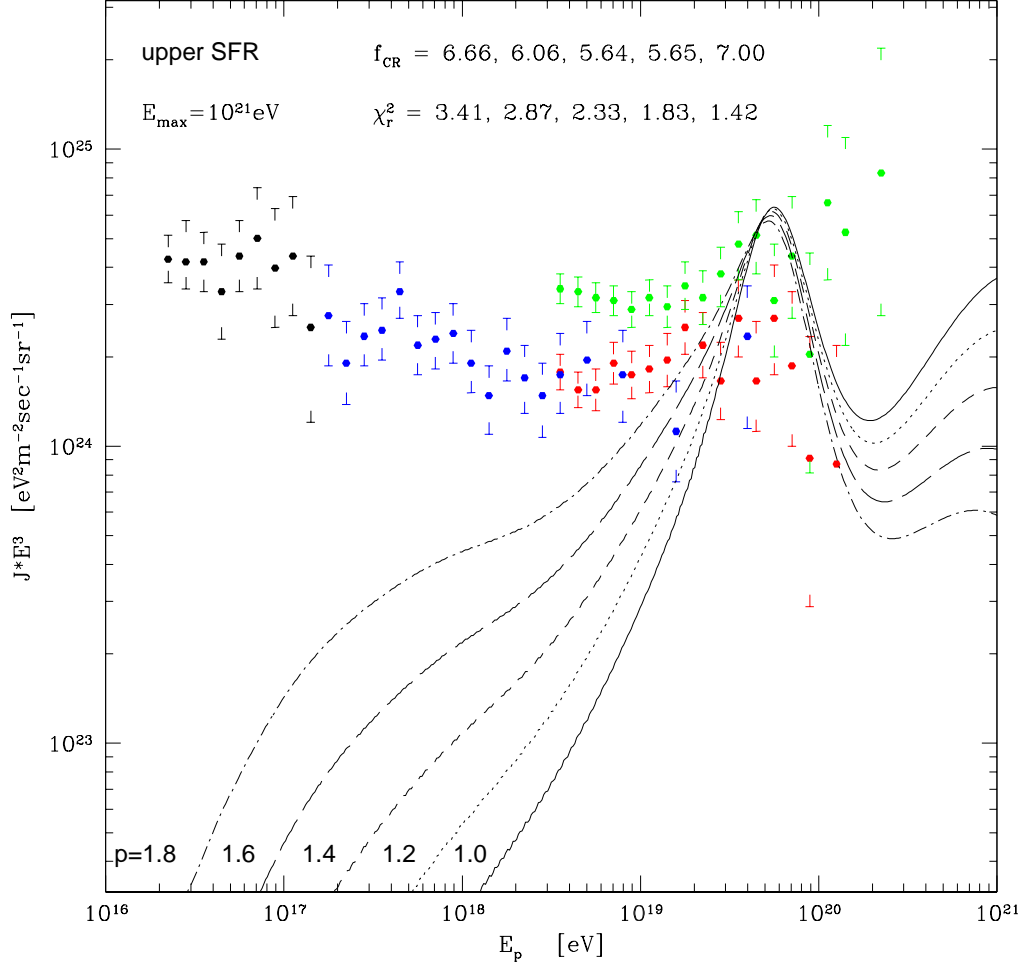


Fig. 11. Best fits to the highest nine energy bins in the AGASA data $3 \times 10^{19} \text{ eV} - 3 \times 10^{20} \text{ eV}$ for various hard spectra, $p = 1.0, 1.2, 1.4, 1.6, 1.8$. The resultant χ_r^2 and requisite baryon loading f_{CR} for each case are shown on the figure. The KASCADE and HiRes data, although shown, are not included in the fits.

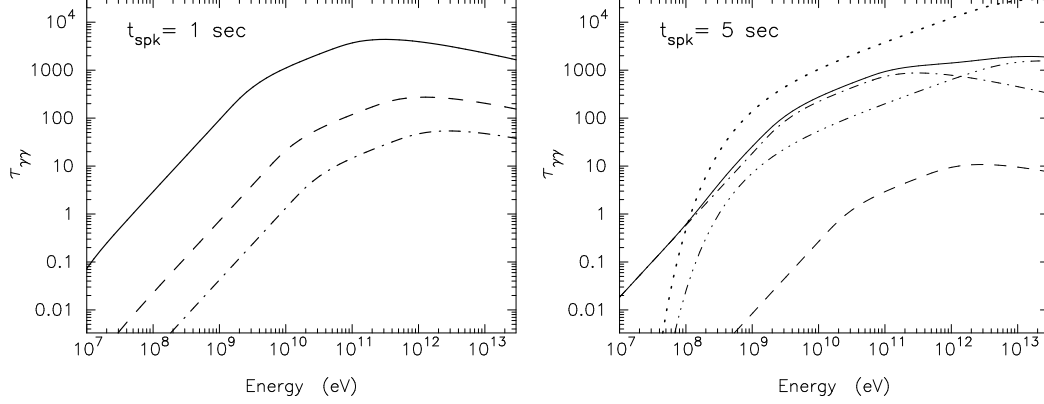


Fig. 12. Opacity $\tau_{\gamma\gamma}$ for gamma-ray absorption in the radiation field inside individual spikes of a GRB at $z = 1$, with the X-ray/MeV gamma ray fluence $\Phi_{rad} = 3 \times 10^{-4} \text{ erg cm}^{-2}$ (with spectral flux peaked at 1 MeV) in the prompt phase with a duration $t_{GRB} = 100 \text{ s}$, calculated for a collapsar GRB **(a)** (*left*): for 3 different Doppler factors $\delta = 100$ (solid curve), 200 (dashed curve), and 300 (dot-dashed curve), assuming that the prompt emission is contributed by $N_{spk} = 50$ individual spikes with the mean duration $t_{spk} = 1 \text{ s}$ each; **(b)** (*right*): for $\delta = 100$ (dot-dashed curve) and 300 (dashed curve), but assuming $N_{spk} = 10$ spikes with the mean duration $t_{spk} = 5 \text{ s}$. For comparison, here we also show contributions to $\tau_{\gamma\gamma}$ due to the external radiation field in the case of “supranova” GRB with the assumed delay between the supernova and GRB events $t_{sd} = 0.3 \text{ yr}$; the 3-dot-dashed curve corresponds to the opacity due to the external photon field, and the solid curve shows the total $\tau_{\gamma\gamma}$, across the spike in the case of $\delta = 100$. The dotted curve shows the opacity across the entire “plerionic nebula” with a radius $\simeq 4.6 \cdot 10^{-3} \text{ pc}$ (see Ref. (35) for details of calculations in the “supranova” scenario).

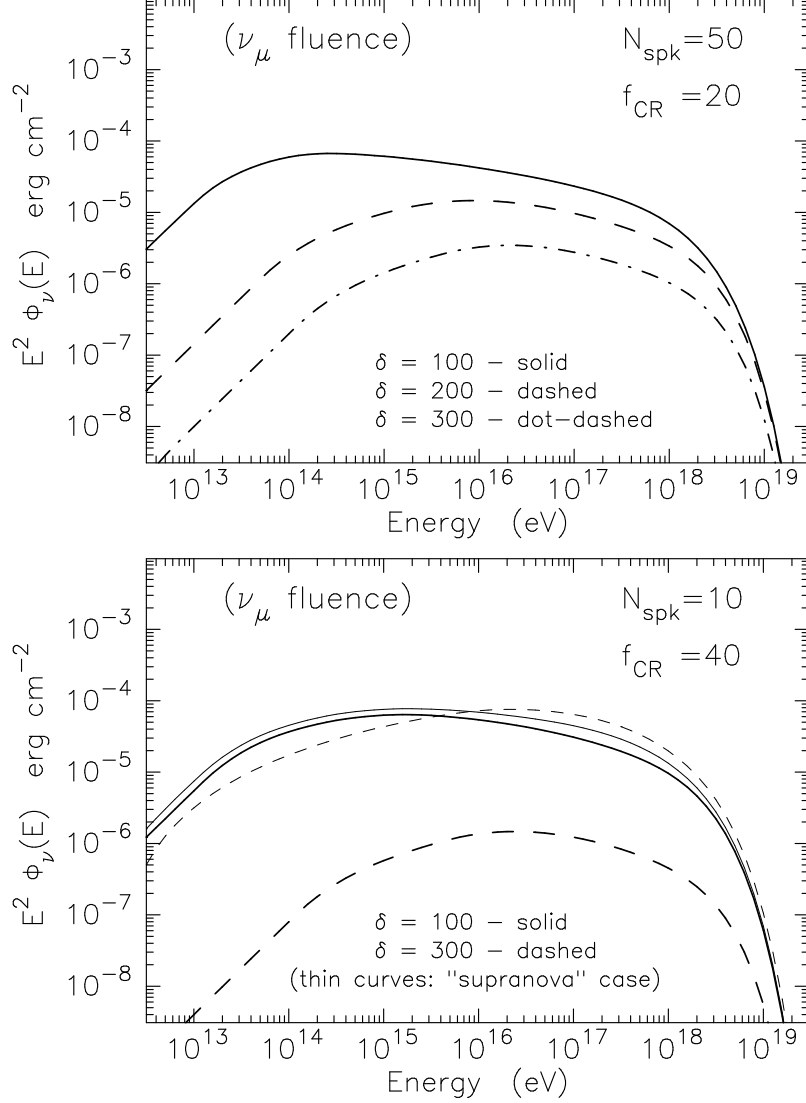


Fig. 13. The fluences of muon neutrinos calculated for a collapsar GRB assuming **(a)** (*top*): 3 different Doppler factors $\delta = 100, 200$ and 300 , the same GRB parameters as in Fig. 12a, and a nonthermal baryon-loading factor $f_{\text{CR}} = 20$; and **(b)** (*bottom*): Doppler factors $\delta = 100$ and 300 , but for the case of $t_{\text{spk}} = 5$ s; for comparison, here we also show by thin curves the fluences expected in the “supranova” model with the same parameters as in Fig. 12b.

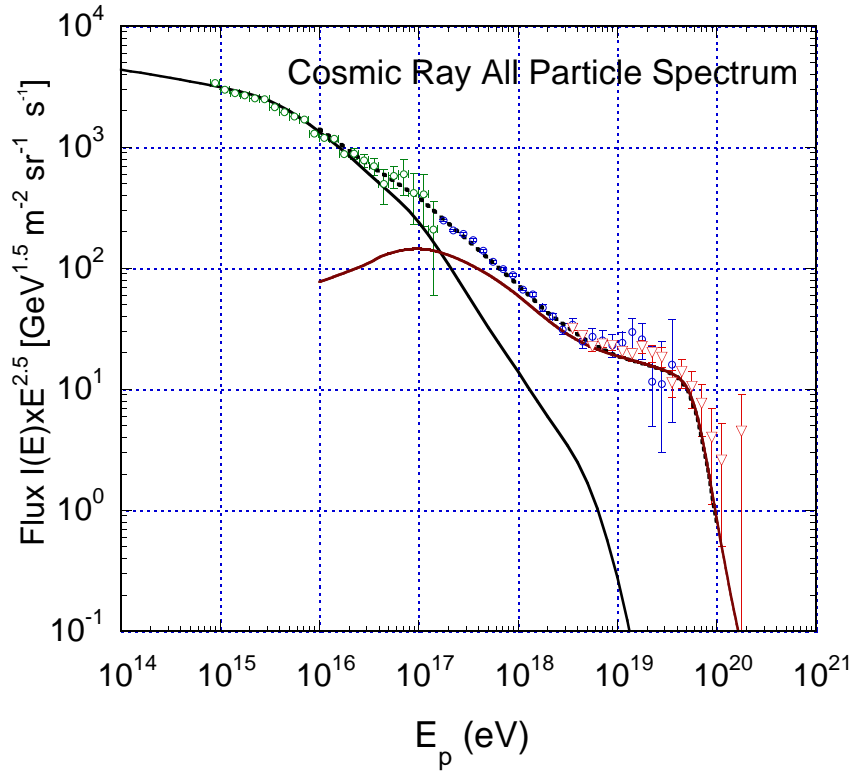


Fig. 14. The all-particle CR data from KASCADE, High-Res I and II, in comparison with the model result for the all-particle spectrum (dotted curve) from galactic (lower energy solid curve) and extragalactic (higher energy solid curve) GRB sources of high-energy cosmic rays.